Periodical
Section

PHYSICAL REVIEW
LETTERS

VOLUME 7 JULY 1, 1961 NUMBER 1

POSSIBILITY OF EXCHANGE MAGNETOSTRICTION YIELDING NEGATIVE THERMAL EXPANSION IN SOLID He^3

D. S. Rodbell
General Electric Research Laboratory, Schenectady, New York
(Received April 10, 1961; revised manuscript received May 24, 1961)

According to Primakoff[1] the nuclear spins of solid He^3 should be antiferromagnetically coupled with a transition temperature that decreases with increasing pressure. The essential features of antiferromagnetism have been observed by Meyer, Adams, and Fairbank[2] to occur in the region of the He^3 phase diagram near 0.1°K for $P>70$ atm. This observation is within order-of-magnitude agreement with the predictions of Bernardes and Primakoff[3-5] and lends support to the exchange interactions so far calculated.[1,3-5] This exchange is believed to be a steep function of lattice parameter[3-5] in the highly compressible ($K \sim 5\times10^{-9}$ cm²/dyne) He^3 lattice. The purpose of this note is to point out that the existence of (a) an exchange interaction dependent upon interatomic separation and (b) a highly compressible lattice are sufficient conditions to give rise to negative thermal expansion behavior. Such behavior has been observed[6] in certain regions of the solid He^3 phase diagram. We outline the features of this mechanism[7] below. Bernardes and Primakoff[5] have shown such behavior to be contained in their spin-wave treatment of the He^3 problem; we believe that the phenomenological approach used here provides some additional physical insight. The physical basis of the mechanism is provided by the fact that the larger the exchange interaction, the lower the system's free energy. Thus a spontaneous distortion in the direction of increasing the exchange will lower the energy but must be paid for with the strain energy of the distorted lattice. In addition a higher effective Curie temperature provides more magnetization at a given temperature and hence lowers the spin entropy.

We now write the Gibbs function ($G=U-TS+PV$) for a spin $\frac{1}{2}$ system and for a volume v_0 as

$$G_{v_0} = \underbrace{-HM_S\sigma\cos(\phi/2)}_{\text{field}} \underbrace{-\tfrac{1}{2}NkT_C\sigma^2\cos\phi}_{\text{exchange}} + \underbrace{\tfrac{1}{2}\left(\frac{v-v_0}{v_0}\right)^2\frac{1}{K}}_{\text{strain}}$$

$$\underbrace{-T(S_{\text{spin}}+S_{\text{lattice}})}_{\text{entropy}} + \underbrace{P\left(\frac{v-v_0}{v_0}\right)}_{\text{pressure}}. \qquad (1)$$

In this expression, H is the magnetic field, M_S the sublattice saturation magnetization, and σ the relative magnetization at temperature T; ϕ is the angle between the assumed sublattices, being 0 for ferromagnetism and π for antiferromagnetism. N is the number of magnetic atoms per unit volume, k is Boltzmann's constant, v is the specific volume, v_0 is the specific volume in the absence of a magnetic interaction, and K is the compressibility. The Curie temperature T_C which we use to measure the exchange interaction in the molecular field approximation is assumed to be given by

$$T_C = T_0\{1+\beta[(v-v_0)/v_0]\}, \qquad (2)$$

where T_0 is the "undistorted" Curie temperature (that may be positive or negative corresponding to ferromagnetism or antiferromagnetism) and β measures the slope of the dependence of T_C/T_0 with specific volume (and may be either positive or negative).

The free energy depends upon the lattice thermal

expansion coefficient, α_l, as this parameter measures the change of lattice entropy with volume. We assume that $S_{\text{latt}} = S_0 + (\alpha_l/K)(v - v_0)$, an expression that is justifiable for a constant α_l but otherwise is simply assumed for this treatment. The spin entropy does not enter directly into the present determination of expression (3) below; it is important in determining $\sigma(T)$, however, and therefore determines the temperature dependence of (3). We have found situations[8] where the spin entropy may dominate a phase transition. The fact that the spin system entropy may play a dominant role has been emphasized by Goldstein[9] and Bernardes and Primakoff[3-5] with regard to solid He^3.

The specific volume that minimizes the free energy (1) is found to be

$$\left.\frac{v - v_0}{v_0}\right|_{\text{equil}} = \alpha_l T - PK + \tfrac{1}{2}NkKT_0\beta\sigma^2\cos\phi. \quad (3)$$

We take T_0 negative, β positive, and in the absence of an external field, $\phi = \pi$ as descriptive of the antiferromagnetic state of He^3.[1-5] The dependence of (3) on temperature is the thermal expansion to be expected in such a system, and in Fig. 1 we indicate the qualitative features of (3) where to the "normal" thermal expansion must be added a term proportional to σ^2. This term disappears with the magnetization as temperature increases and results in the possibility of a change in sign of the thermal expansion coefficient. The necessary condition for negative thermal expansion behavior is that $\alpha_l < \frac{3}{2}NKk\beta$ be true.[10] This is indeed the case for solid He^3 using the measured values of (α_l, K)[6,11] and with $(1/T_c)(\partial T_c/\partial P) \sim 10^{-2}$ from Bernardes and Primakoff[5] which corresponds to $\beta = 2$.

If the exchange energy vs lattice parameter has a monotonic dependence, then the distortion that in the antiferromagnetic state favors an expanded lattice will in the ferromagnetic state become a contraction, since this provides the largest absolute values of T_c (hence the lowest free energy) in each case. These views would argue in favor of a denser ferromagnetic solid than an antiferromagnetic one and would suggest that the exchange energy and its dependence upon atomic separation directly contributes to the phase change that yields a denser solid at high pressure, as has been observed. The latter conclusion supports recent suggestions by Bernardes and Primakoff.[5] The detailed treatment[8] of the problem outlined here also evaluates the "magnetic phase diagrams" of such systems and finds possible first- and second-order phase transitions occurring as pressure or temperature are varied. The predictions by Bernardes[12] and Primakoff[5] of a transition from antiferromagnetism to ferromagnetism[13,14] with an external pressure of 200 atmospheres or greater (near 0.1°K) is in accord with our own "model" using Bernardes' and Primakoff's value for β; in addition we would also predict a range of temperatures where transitions from antiferromagnetism → paramagnetism → ferromagnetism would occur with increasing pressure. This last feature may have bearing upon the unusual susceptibility behavior that has been observed.[2]

In conclusion, it should be noted that a depend-

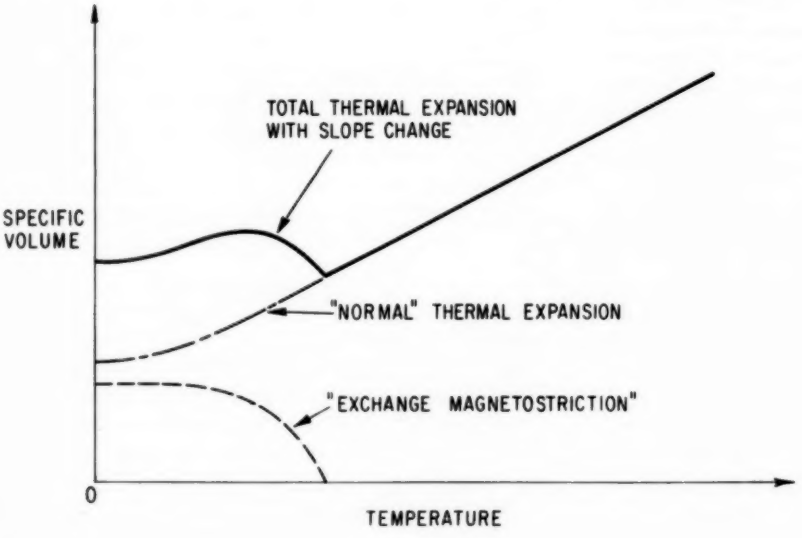

FIG. 1. The total thermal expansion of a highly compressible lattice with exchange interaction as described in the text.

ence of exchange on lattice parameter of opposite sign (β negative) would not yield (for an antiferromagnetic ground state) negative thermal expansion behavior since the exchange magnetostriction term would give rise to a contraction at $T=0$. It may thus be that the observation of negative thermal expansion in solid He^3 is auxiliary evidence for the supposed dependence of exchange upon lattice parameter.

I have benefited from communications with Professor H. Primakoff on the subject of this note, the kernel of which originated in a more general problem on magnetic phase transitions done in conjunction with C. P. Bean.

[1]H. Primakoff, Bull. Am. Phys. Soc. 2, 63 (1957).

[2]H. Meyer, E. D. Adams, and W. M. Fairbank, Proceedings of the Seventh International Conference on Low-Temperature Physics, September, 1960 (University of Toronto Press, Toronto, 1960), p. 339.

[3]N. Bernardes and H. Primakoff, Phys. Rev. Letters 2, 290 (1958).

[4]N. Bernardes and H. Primakoff, Phys. Rev. Letters 3, 144 (1959).

[5]N. Bernardes and H. Primakoff, Phys. Rev. 119, 968 (1960).

[6]E. Grilly, S. Sydoriak, and R. Mills, in Helium 3, edited by J. G. Daunt (Ohio State University Press, Columbus, Ohio, 1960).

[7]C. P. Bean and D. S. Rodbell, Bull. Am. Phys. Soc. 6, 159 (1961).

[8]C. P. Bean and D. S. Rodbell (to be published).

[9]L. Goldstein, Ann. Phys. 8, 390 (1959).

[10]This condition results from evaluating $|\sigma d\sigma/dT|$ at its maximum ($\sigma \to 0$) from the Brillouin function for $j=1/2$ where $\lim_{\sigma\to 0}|\sigma d\sigma/dT| = 3/2T_0$. The effect of modifying the Brillouin function as occurs in this treatment will raise this value; we have therefore evaluated the lower bound of this exchange magnetostriction.

[11]Estimating α_l from the high-temperature measurements to be less than 10^{-2}/°K while $K \sim 5\times10^{-9}$ cm²/dyne.

[12]N. Bernardes, in Helium 3, edited by J. G. Daunt (Ohio State University Press, Columbus, Ohio, 1960).

[13]A transition of this type may be appreciably affected by externally applied magnetic fields and may be understood through the magnetic analog of the Clausius-Clapeyron relation, e.g., $\Delta T/T = H\Delta M/L$; for latent heat, L, a transition temperature change ΔT will result for an applied field H; ΔM is the difference in net magnetization per unit volume between the ferromagnetic and antiferromagnetic states. If the latent heat is largely due to changes in the spin system entropy, then L may be small and ΔT large.

[14]Note added in proof. M. J. Klein and R. D. Mountain [Phys. Rev. Letters 5, 363 (1960)] have pointed out that the thermal expansion must change sign when the transition from antiferromagnetism to ferromagnetism occurs. This is also evident in our Eq. (3) when ϕ changes from π to 0.

FLUX AND ENERGY SPECTRA OF THE PROTONS IN THE INNER VAN ALLEN BELT

J. E. Naugle and D. A. Kniffen

National Aeronautics and Space Administration, Goddard Space Flight Center, Greenbelt, Maryland

(Received June 8, 1961)

In this experiment, for the first time, the flux and energy spectrum of the trapped protons in the inner Van Allen belt were measured as a function of position in the belt. Previous measurements[1,2] of the proton energy spectrum have been made in emulsions which integrated over the entire flight paths of intercontinental ballistic missiles flown from Cape Canaveral.

On September 19, 1960, a research rocket with a special nose cone developed for the exposure and recovery of emulsions was flown along a trajectory which closely corresponded to a magnetic meridian. The rocket payload was designed to permit a four-inch cylinder to be extended out through the front end of the nose cone, thereby reducing the amount of material surrounding the emulsion container to a minimum. Time resolution of the spectrum was obtained by exposing sections of a cylindrical emulsion stack to the ambient radiation through a port in the tungsten emulsion container. Figure 1 shows the experimental arrangement. A point on the periphery of the stack was behind the port for approximately 80 seconds. During the rest of the flight that point was shielded by 30.6 g/cm² of tungsten. Therefore, the track population at such a point is made up of particles which came in through the port during the 80-second exposure and a background of particles which passed through the tungsten during the remaining 900 seconds the payload was in flight. A portion of the stack which did not pass behind the port has been used to measure the background. Protons of energy ≥ 8 Mev were able to penetrate

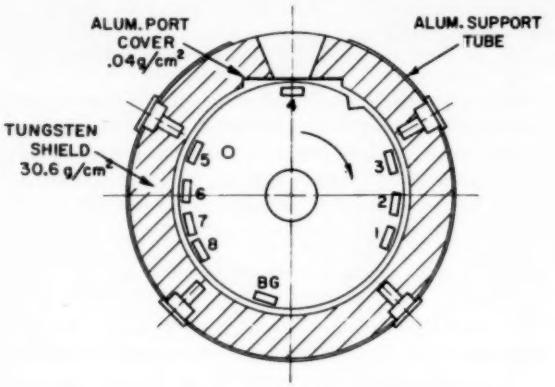

FIG. 1. Film position at apogee. 25 circular G-5 and G-0 nuclear emulsions were contained in a tungsten cassette. The numbered points around the periphery of the stack refer to the sections of the emulsion which are being analyzed.

the aluminum port cover and be detected, whereas only protons with $E \geq 145$ Mev were recorded in the emulsion after passing through the tungsten shield.

Figure 2 shows the trajectory of the rocket payload. The numbered points along the trajectory indicate the locations at which the corresponding points on the stack were behind the port. Table I gives the pertinent data regarding the three points 3, 4, 5, which have been analyzed to date.

A "line scan" was made around the periphery of the emulsions at points 3, 4, and 5. The scan was made approximately 500 microns from the edge of the emulsions. It was not possible to scan closer to the edge of the emulsion because of blackening. All particles which, at the scan line, were within ±25° of a radius vector and ±45° of the plane of the emulsion were recorded.

The portion of the emulsion which was not exposed behind the port was also scanned, with the same criteria, to obtain an integral flux averaged over the entire flight and also to obtain a background correction for the other sections of the stack.

In order to obtain the differential energy spectrum, all particles in the scans which had a possible residual range in the emulsion, at the scan line, of at least 2.5 mm were followed until they either ended, interacted, or left the stack. The energies and mass of these particles were then determined from range, ionization, and scattering measurements.

In the analysis to date, no evidence has been found for particles other than protons crossing the scan line. However, the mass measurements do not rule out a small component of singly-charged particles heavier than protons. The thickness of the blackened edge of the emulsion varies around the periphery of the stack and is consistent with electrons of energy up to about 600 kev stopping in the emulsion. There is a high background of grains for another 500 microns in from the black edge, due possibly to the presence of soft x rays.

The number of protons with energy greater than 100 Mev crossing the scan lines was ap-

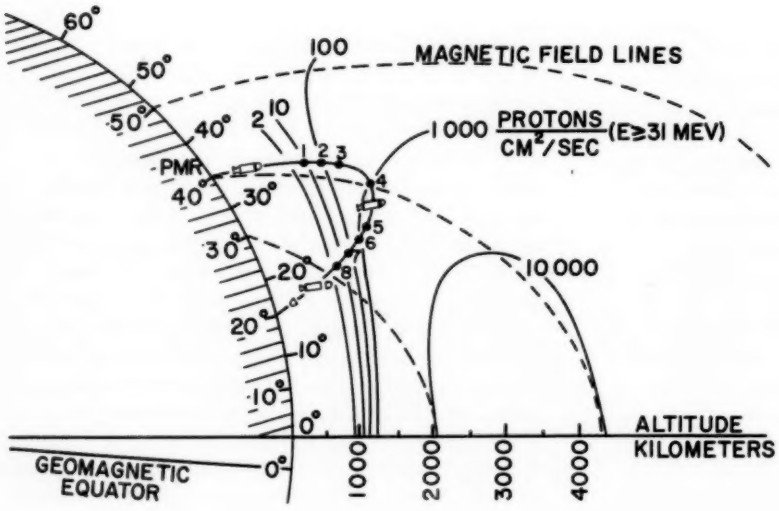

FIG. 2. Meridian section of the earth showing the trajectory of the rocket payload relative to the magnetic field and the radiation belt.

Table I. Summary of results.

Point 3:

1600 km
28.4°N lat.
237.7°W long.
$B = 0.231$ gauss
$I = 1.67\, r_e$

$J(E \geq 31) = 70 \pm 15$ protons/cm^2 sr sec
$4\pi J(E \geq 31)_a = 900 \pm 200$ protons/cm^2 sec
$J_0(E \geq 31) = 220$ protons/cm^2 sec

$J(E) = (3.2 \pm 0.6) \times 10^6 / E^{4.5 \pm 0.5}$ protons/cm^2 sec sr Mev; $10 \leq E \leq 50$ Mev

Point 4:

1884 km
25.2°N lat.
236.5°W long.
$B = 0.198$ gauss
$I = 1.34\, r_e$

$J(E \geq 31) = 120 \pm 20$ protons/cm^2 sr sec
$4\pi J(E \geq 31)_a = 1500 \pm 250$ protons/cm^2 sec
$J_0(E \geq 31) = 1000$ protons/cm^2 sec

$J(E) = (6.8 \pm 0.3) \times 10^6 / E^{4.5 \pm 0.2}$ protons/cm^2 sec sr Mev; $10 \leq E \leq 50$ Mev

Point 5:

1600 km
21.5°N lat.
235.4°W long.
$B = 0.209$ gauss
$I = 0.946\, r_e$

$J(E \geq 31) = 190 \pm 40$ protons/cm^2 sr sec
$4\pi J(E \geq 31 \text{ Mev})_a = 2400 \pm 500$ protons/cm^2 sec
$J_0(E \geq 31 \text{ Mev}) = 1290$ protons/cm^2 sec

$J(E) = (1 \pm 0.5) \times 10^3 / E^{1.7 \pm 0.3}$ protons/cm^2 sec sr Mev; $40 \leq E \leq 100$ Mev

Integral flux behind 30.6 g/cm^2 of tungsten, averaged over trajectory.

$J(E \geq 145 \text{ Mev}) = 16 \pm 3$ protons/cm^2 sr sec

[a]Integral omnidirectional proton flux at point based on satellite data.[5]

proximately equal to the number in the background area in the same energy range. Therefore, it is not possible, with the statistics available at this time, to make reliable measurements of the spectrum above about 100 Mev.

The spectra obtained at the three points are shown in Fig. 3.

Three things are apparent from these results: (1) At the higher latitudes, the slope of the spectrum below 40 Mev is very steep compared to

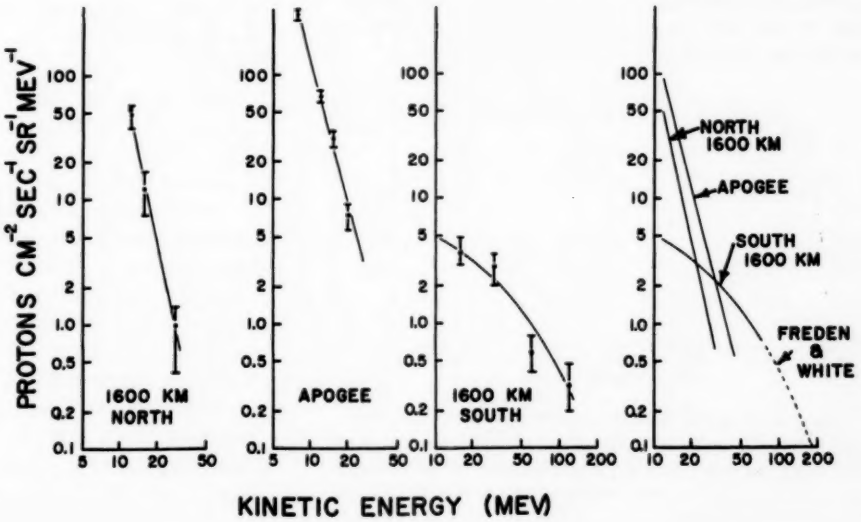

FIG. 3. The differential energy spectra obtained at points 3, 4, and 5 on the trajectory, together with the three spectra superimposed for purposes of comparison.

predictions from galactic cosmic-ray neutron albedo theory.[3] (2) The shape of the spectrum and the flux change with latitude. Points 3 and 5 are at the same altitude and geomagnetic longitude. (3) At a comparable position in the belt (point 5) the flux and shape of the spectrum agree with the previous data.

Singer[4] has predicted a change in the slope of the spectrum at higher energies with a change in latitude based on the assumption that the maximum energy of the trapped protons decreases with altitude due to the breakdown of the adiabatic invariance of the magnetic moment. It is also possible that the change in the spectrum at lower energies is due either to solar protons trapped in the geomagnetic field or to protons produced by the decay of albedo neutrons produced in nuclear interactions of solar protons over the polar cap. In either case there would be a preferential trapping of low-energy particles at the higher latitudes.

It is not clear which of these mechanisms is responsible for the change in the spectrum. Further analysis will be made in these emulsions to determine the maximum energy at which protons can be trapped at a given point. Additional flights are scheduled in late 1961 to determine if there is a time variation. Assuming that the low-energy protons are associated with solar activity, their flux should decrease as the number of solar proton events per year decreases during the solar cycle. Changes in the spectrum after a large flare have been reported by Armstrong et al.[2]

The unidirectional integral flux, J, for protons with $E \geq 31$ Mev is given in Table I. In order to compare this flux with the measurements in satellites, the assumption has been made that the flux is isotropic so that the integral omnidirectional flux is obtained by multiplying J by 4π. The values obtained in this way are listed in Table I together with the best value of the flux at the three points based on the analysis of the satellite data.[5] The quoted errors are large due to the effects of the background on the integral flux. The agreement is quite good considering the errors. The unidirectional flux, assuming isotropy, is consistently higher than the omnidirectional flux at all three points, indicating that the assumption is not valid.

The nose cone was spin stabilized nearly parallel to the magnetic field lines, and the unidirectional flux in the emulsion was measured primarily at angles near 90° with respect to the field lines. At low altitudes, where there is a high density of mirror points, the flux should not be isotropic but should be higher at 90° angles as observed.

The solution of the problems associated with the exposure and recovery of emulsions at 1880 km required outstanding and unique contributions from a number of people. These efforts are gratefully acknowledged by the authors. In particular, the shot would not have been successful without the work over and above his normal responsibility by Project Engineer Charles E. Campbell, of the Goddard Space Flight Center.

---

[1] S. C. Freden and R. S. White, Phys. Rev. Letters 3, 9 (1959).

[2] A. H. Armstrong, F. B. Harrison, H. H. Heckman, and L. Rosen, J. Geophys. Research 66, 351 (1961).

[3] S. C. Freden and R. S. White, J. Geophys. Research 65, 1399 (1960); S. F. Singer, Phys. Rev. Letters 1, 141, 181 (1958); W. N. Hess, Phys. Rev. Letters 3, 11 (1959).

[4] S. F. Singer, Space Research (Interscience Publishers, Inc., New York, 1960), p. 797.

[5] C. E. McIlwain and J. A. Van Allen (private communication).

FERROMAGNETISM IN SOLID SOLUTIONS OF SCANDIUM AND INDIUM

B. T. Matthias, A. M. Clogston, H. J. Williams, E. Corenzwit, and R. C. Sherwood
Bell Telephone Laboratories, Murray Hill, New Jersey
(Received June 12, 1961)

We have found that a solid solution of approximately 24 atomic percent indium in scandium becomes ferromagnetic below 6°K. The ferromagnetism occurs over an extremely narrow range of compositions between $Sc_{0.762}In_{0.238}$ and $Sc_{0.758}In_{0.242}$, a change of 0.4 atomic percent of indium.

The ferromagnetism of these solid solutions was encountered during a search for superconductivity in the scandium-indium system. After the discovery that La_3In becomes superconducting at 10.4°K,[1] the corresponding phases of yttrium and scandium became of interest. While In is not soluble in Y, no difficulty has been found in dissolving In in Sc simply by melting the materials together in an arc furnace. Measurements of the susceptibility of these melts initially showed a maximum near 20 atomic percent In. After the ingots were annealed for a week at 800°C the maximum susceptibility increased greatly and moved to higher In concentrations. No superconductivity has been found in this system. X-ray patterns do not show the cubic La_3In phase but instead the essentially hexagonal close-packed symmetry of scandium metal, with a smaller lattice constant, consistent with a smaller atomic radium for metallic indium than for scandium. At the composition $Sc_{0.70}In_{0.30}$ the structure changes.

In Fig. 1 we show a plot of the magnetic moment in cgs units per gram observed in a field of 14 000 gauss at 1.4°K as a function of the atomic fraction of In for the annealed samples. The extreme sharpness of the peak shows how very easy it would be to miss the occurrence of ferromagnetism in this system. Measurements have been made of the susceptibilities χ for these solid solutions from 1.4°K to room temperature. χ is strongly temperature dependent, becoming large at low temperatures, and can be fitted approximately to a Curie-Weiss law of the form $\chi = N\mu_B^2 p_{eff}^2/3k(T-\theta)$ where N is the number of magnetic centers, μ_B is the Bohr magneton, p_{eff} is the effective magnetic moment per atom, and θ is the Curie temperature. The values of p_{eff} and θ are shown as a function of composition in Figs. 2 and 3 and in Table I. Although p_{eff} shows a small peak at the critical composition, the large peak in the mag-

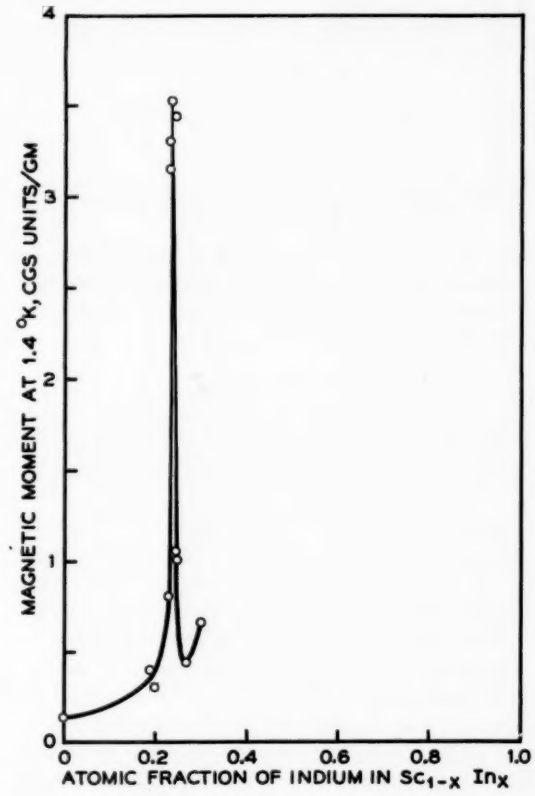

FIG. 1. Magnetic moment per gram observed at 1.4°K in a field of 1400 gauss with a sample of $Sc_{1-x}In_x$ as a function of atomic fraction of In.

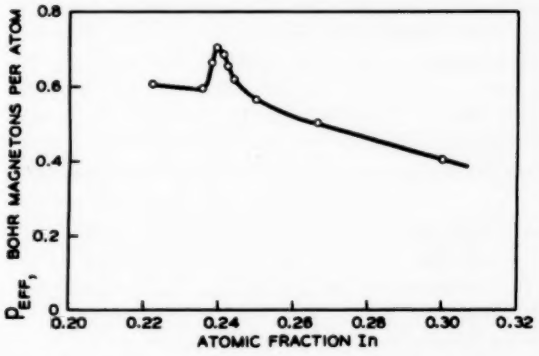

FIG. 2. Effective magnetic moment in Bohr magnetons per atom for $Sc_{1-x}In_x$ as a function of atomic fraction of In, determined by fitting observed susceptibilities to a Curie-Weiss law.

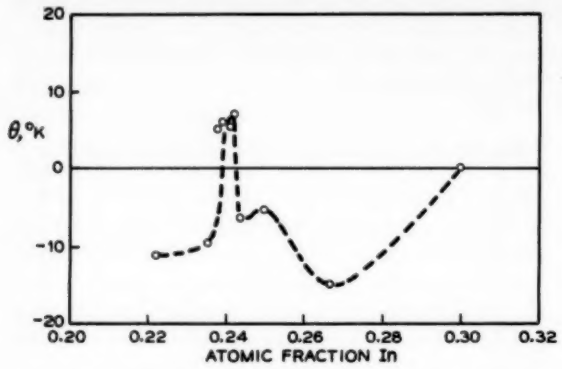

FIG. 3. Curie-Weiss constant θ in degrees Kelvin of of a sample of $Sc_{1-x}In_x$, as a function of atomic fraction of In, determined by fitting observed susceptibilities to a Curie-Weiss law.

netic moment shown in Fig. 1 clearly arises from the fact that θ becomes positive at this point. The accuracy in determining θ is not better than 1 or 2°K.

A positive value of θ implies that the material must become ferromagnetic for $T < \theta$. For the four samples where θ is positive, the magnetic moment has been studied as a function of H and T. The Curie temperature T_C has been determined by plotting H/σ_g vs σ_g^2 isotherms, where σ_g is the magnetization per gram. These results are given in Table II along with the saturation moment μ_a per atom in Bohr magnetons. We also show the magnetic moment per atom determined from the Curie-Weiss law assuming $g=2$. Remanence has been observed at 1.4°K.

The nature of the ferromagnetic state in $Sc_{0.76}In_{0.24}$ is not clear at this point. The Curie-Weiss law obeyed by the susceptibilities suggests that the scandium d electrons are partially localized and exhibit a small magnetic moment.

Table I. θ and p_{eff} for $Sc_{1-x}In_x$ as a function of x.

x	p_{eff}	θ°K
0.222	0.60	-11
0.235	0.60	-10
0.238	0.66	+5
0.240	0.70	+6
0.241	0.69	+6
0.242	0.65	+7
0.244	0.62	-6
0.250	0.56	-5
0.267	0.50	-15

If this were the case we would have a ready explanation of the fact that no superconductivity develops in this system in contrast to the high superconducting transition temperature of La_3In. This model, however, provides no explanation why ferromagnetism should appear in such an extremely narrow range of compositions.

The sensitivity to composition and homogeneity is perhaps suggestive of a band-filling mechanism, leading to itinerant electron ferromagnetism. A similar situation has been reported previously for $ZrZn_2$,[2] which becomes ferromagnetic below 35°K.

In this case, Abrahams[3] could not detect the 1.4 Bohr magnetons per atom indicated by the Curie-Weiss law although his measurements were consistent with the smaller value of 0.17 μ_B determined by measurements of the saturation magnetization. Electrical resistivity measurements by Olsen[4] also failed to show any spin disorder scattering above the Curie temperature. The ferromagnetism of $ZrZn_2$ is easily destroyed by impurities and other lattice disturbances.

An attempt to account for the ferromagnetism of the Sc-In system by an itinerant electron model, however, also faces difficulties. It is easy to show that the susceptibility of the band model above the Curie temperature will be given, in the Hartree-Fock approximation, by the expression

$$\frac{1}{\chi} = \frac{1}{\chi_0(T)} - \frac{\Omega}{2\mu_B^2} J, \qquad (1)$$

where $\chi_0(T)$ is the temperature-dependent susceptibility that would prevail in the absence of exchange, Ω is the atomic volume, and J is approximately the exchange self-energy of an electron on one lattice site. If the band in question is fairly wide, $\chi_0(T)$ and χ will be essentially temperature independent, contrary to our observations. If the band is narrow enough to introduce substantial temperature variations in $\chi_0(T)$, it will still be difficult to match the shape of the observed susceptibility curves using Eq. (1) since experimental-

Table II. T_C and μ_a for $Sc_{(1-x)}In_x$ as a function of x.

x	T_C°K	μ_a(Bohr magnetons)	$(1+p_{eff}^2)^{1/2}-1$
0.238	5	0.035	0.20
0.240	6	0.036	0.22
0.241	6	0.039	0.22
0.242	6	0.038	0.18

ly χ is rising sharply at the lowest temperatures.

The narrow range of compositions for which ferromagnetism exists in the Sc-In system suggests that this kind of ferromagnetism may be a more general phenomenon than has been thought until now, and may be found to occur in other systems.

We would like to thank Mrs. V. B. Compton for her x-ray investigations of these alloys.

[1]B. T. Matthias, V. B. Compton, and E. Corenzwit, J. Phys. Chem. Solids 19, 130 (1961).

[2]B. T. Matthias and R. M. Bozorth, Phys. Rev. 109, 604 (1958).

[3]S. C. Abrahams, Z. Krist. 112, 427 (1959).

[4]C. E. Olsen, J. Phys. Chem. Solids 19, 660 (1961), and to be published.

SHIFT OF NUCLEAR QUADRUPOLE RESONANCE FREQUENCY BY ELECTRIC FIELD

Toshimoto Kushida* and Kuniomi Saiki†

Hiroshima University, Hiroshima, Japan

(Received June 14, 1961)

It is well known that a static magnetic field splits the nuclear quadrupole resonance (NQR) lines in a single crystal.[1] One might immediately think of the similar effect caused by an electric field applied to the specimen. As a matter of fact, Pound[2] applied a field of about 50 000 v/cm across a thin plated-shaped single crystal of potassium iodide, but no shift in the resonance frequency nor change in the line shape was observed in the I^{127} nuclear resonance line. Gutowsky and Williams[3] tried to observe the effect of an electric field on an NQR line of the Cl nucleus in $NaClO_3$ single crystal without success.

Recently Bloembergen[4] pointed out the possibility of observing the change in the quadrupole coupling constant caused by an external electric field, if the crystal lattice has no local inversion symmetry about the pertinent nucleus.

It is the purpose of this Letter to report the successful observation of this effect for the Br^{81} NQR line in a single crystal of $NaBrO_3$.[5] The resonance frequency and the line shape are observed as a function of applied electric field using a regenerative spectrometer[6] in conjunction with a precise 0°C ice bath in order to keep the temperature of the sample constant during the run. Aluminum film electrodes are evaporated on the surfaces of a thin plate sample which has been cut from a larger single crystal.

The peak frequency of the line shifts linearly with the applied field E when E is parallel to [111], whereas no shift in the center frequency is observed in the case of $E \parallel [100]$. Reversal of the polarity of E reverses the sign of the shift. A typical example of the observed absorption curve is shown in Fig. 1. Here E is along the

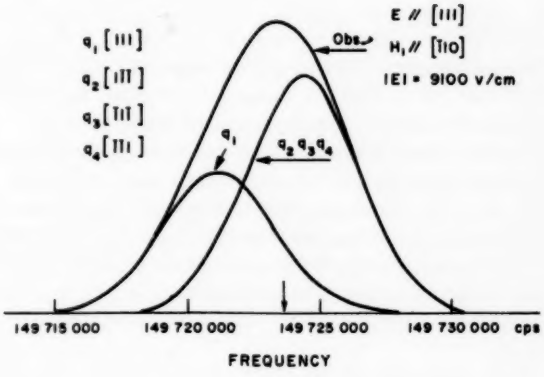

FIG. 1. The effect of the electric field on the Br^{81} resonance in $NaBrO_3$ single crystal. The arrow ↓ indicates the center frequency of the original line without the field.

[111] direction of the crystal, and H_1, an rf magnetic field in a sample coil of the spectrometer, is applied along the [1̄10] direction. The vertical arrow ↓ indicates the center frequency without the electric field. The line shape, which was symmetric without an E field, is slightly asymmetric, and the center frequency has shifted by about 500 cps.

A cubic unit cell[7] of $NaBrO_3$ has four physically inequivalent, but chemically equivalent, BrO_3^- radicals. The maximum principal axes of electric field gradients about Br nuclei are parallel to the body diagonals of the unit cell. The field gradients along the [111], [1$\bar{1}\bar{1}$], [$\bar{1}$1$\bar{1}$], and [$\bar{1}\bar{1}$1] directions will be denoted, respectively, by q_1, q_2, q_3, and q_4.

The distortions of the field gradients produced

by the electric field along [111] are the same for q_2, q_3, and q_4 because of the threefold symmetry of the crystal along this direction. Because q_1 distorts differently, a doublet separation of the line would be expected. Since the relative intensity of the component lines is proportional to $\sin^2\angle(H_1, q)$, the intensity ratio of the components of the doublet will be $I_1:I_{234}=3:5$ in the case of $H_1 \| [\bar{1}10]$. Using this intensity ratio the observed asymmetric curve can be decomposed into two components as shown in Fig. 1. When H_1 is along the [111] direction, one observes only the $(q_2q_3q_4)$ line, which does not show any asymmetry nor increase in the linewidth compared with the original line without the E field. The observed shift of each component is

q_1 line $\quad -2500 \pm 500$ cps/(10 000 v/cm),

$(q_2q_3q_4)$ line $\quad 750 \pm 150$ cps/(10 000 v/cm).

The minus sign for the q_1 line indicates only the fact that the q_1 and the $(q_2q_3q_4)$ lines shift to opposite directions; no attempt has made to determine the absolute sign of these magnitudes.

When E is along [100] and H_1 is along [010], the shift for the (q_1q_2) line is the same as, but opposite in sign to, that for the (q_3q_4) line. Since both lines have the same intensity, no shift in the center frequency is observed up to about 5000 v/cm, where the crystal always breaks down.

The distortion of the field gradient tensor component, $\delta\varphi_{ij}$, may be expressed as

$$\delta\varphi_{ij}=\sum_k(\partial\varphi_{ij}/\partial E_k)E_k; \quad i,j,k=x,y,z. \qquad (1)$$

The third rank tensors, $\partial\varphi_{ij}/\partial E_k$, are zero if local inversion symmetry about the nuclei exists. This is the case for KI. Symmetry requirements of the crystal structure[8] and the traceless property[1] of φ_{ij} generally decrease the number of the independent components of this tensor.

The observed shift of the resonance frequency indicates only the change in q, which is φ_{ii} along the maximum principal axis, because a small asymmetry parameter η produced by the E field changes the resonance frequency only in the second order. From the shift of the q_1 line we obtain

$$\delta\nu_{q_1}/\nu_0=(q_0^{-1}\partial q/\partial E_{\|})E, \qquad (2)$$

and the shift of the $(q_2q_3q_4)$ line gives

$$\delta\nu_{q_2q_3q_4}/\nu_0=(q_0^{-1}\partial q/\partial E_{\perp})\frac{2\sqrt{2}}{3}E-(q_0^{-1}\partial q/\partial E_{\|})\frac{E}{3}, \qquad (3)$$

where ν_0 and q_0 are, respectively, the original resonance frequency and q without the field.

The values of the "field-gradient electrostatic" tensor are derived as

$$q_0^{-1}\partial q/\partial E_{\|}=(1.7\pm0.3)\times10^{-5}/(10\,000 \text{ v/cm}), \qquad (4)$$

and

$$q_0^{-1}\partial q/\partial E_{\perp}=(0.0\pm0.2)\times10^{-5}/(10\,000 \text{ v/cm}). \qquad (5)$$

The vanishing of $\partial q/\partial E_{\perp}$ is expected from the symmetry requirements of the third rank tensor for this crystal.[4,9]

Since $NaBrO_3$ is piezoelectric,[8] it would be informative to compare the value of $q_0^{-1}\partial q/\partial E_{\|}$ with the q change produced by a piezoelectric strain. The electric field along the [111] direction produces an axial strain along this direction.[8] The resonance frequency change accompanying this axial strain can be estimated from the piezoelectric constant and the pressure (hydrostatic) dependence of the resonance frequency.[10] Since the implicit effect via the piezoelectric strain thus estimated is less than 10% of the observed value of $q_0^{-1}\partial q/\partial E_{\|}$, it may be concluded that the explicit electric effect on q, namely $(q_0^{-1}\partial q/\partial E_{\|})_{\text{const strain}}$, is mainly responsible for the observed effect.

The authors are indebted to Professor N. Bloembergen for valuable discussions and to Dr. A. H. Silver for the critical reading of the manuscript.

---

*Present address: Scientific Laboratory, Ford Motor Company, Dearborn, Michigan.

†Research Laboratory, Nippon Leather Company, Senju, Tokyo, Japan.

[1]For instance, T. P. Das and E. L. Hahn, Solid State Physics, edited by F. Seitz and D. Turnbull (Academic Press, Inc., New York, 1958), Suppl. 1.

[2]R. V. Pound, Phys. Rev. 79, 685 (1950).

[3]H. S. Gutowsky and G. A. Williams, Phys. Rev. 105, 464 (1957).

[4]N. Bloembergen, Science 133, 1363 (1961).

[5]T. Kushida and K. Saiki, Abstracts of papers presented at the Physical Society Meeting of Japan, April, 1961, Tokyo, Japan (Japanese) (unpublished).

[6]G. B. Benedek and T. Kushida, Phys. Rev. 118, 46 (1960).

[7]R. W. G. Wyckoff, Crystal Structure (Interscience Publishers, Inc., New York, 1951), Vol. II.

[8]For instance, W. P. Mason, Piezoelectric Crystals and Their Application to Ultrasonics (D. Van Nostrand Company, Inc., New York, 1950), p. 41.

[9]The authors are grateful to Professor N. Bloembergen for pointing out this property.

[10]T. Fuke (private communication).

LINEAR EFFECT OF APPLIED ELECTRIC FIELD ON NUCLEAR QUADRUPOLE RESONANCE*

J. Armstrong, N. Bloembergen, and D. Gill
Gordon McKay Laboratory, Harvard University, Cambridge, Massachusetts
(Received June 14, 1961)

Experimental evidence for the existence of a linear Stark effect which was predicted theoretically by one of us,[1] has been found in the zero-field quadrupole resonance of Cl^{35} in $KClO_3$ and $NaClO_3$. Kushida[2] has independently, and somewhat earlier, discovered the same effect for the Br^{81} resonance in $NaBrO_3$.

Because single crystals were not immediately available, our experiments have been carried out with powders of fine crystallites, which filled the 1.68-mm wide spacings between a sandwich of condenser plates. The tank coil of a modified Pound spectrometer,[3] consisting of a few turns of copper ribbon, was wound around the electrostatic condenser assembly and placed in liquid nitrogen. A dc voltage of up to 3500 volts could be applied without causing electrical breakdown. This corresponds to an average field strength in the crystallites of about 17.1 kv/cm. This value was determined from approximate formulas for the inhomogeneous medium[4] with the known powder filling factor of 0.63.

The frequency of the spectrometer was swept linearly through the resonance, which occurs at 28 954 Mc/sec for $KClO_3$ at 77°K. A frequency modulation at 340 cps with a modulation index less than 0.25 was used.[5] The signal output of the phase-sensitive detector corresponds to the absorption derivative of the zero-field quadrupole resonance. Two recorded traces for $KClO_3$, one without electric field and one with 3000 volts between the condenser plates, are shown in Fig. 1. The marked variation in line shape is striking. From such reproducible recordings the increase in second moments as a function of the applied electric field was calculated. The results in Table I show that the second moment increases linearly with the electrical energy stored in the crystallites.

The theoretical interpretation of these results is based on a linear variation of the electric field gradient at the position of the nuclei with the externally applied electric field, if these positions lack inversion symmetry. This relationship can be described by a third order tensor with components R_{ijk}. The variation in field

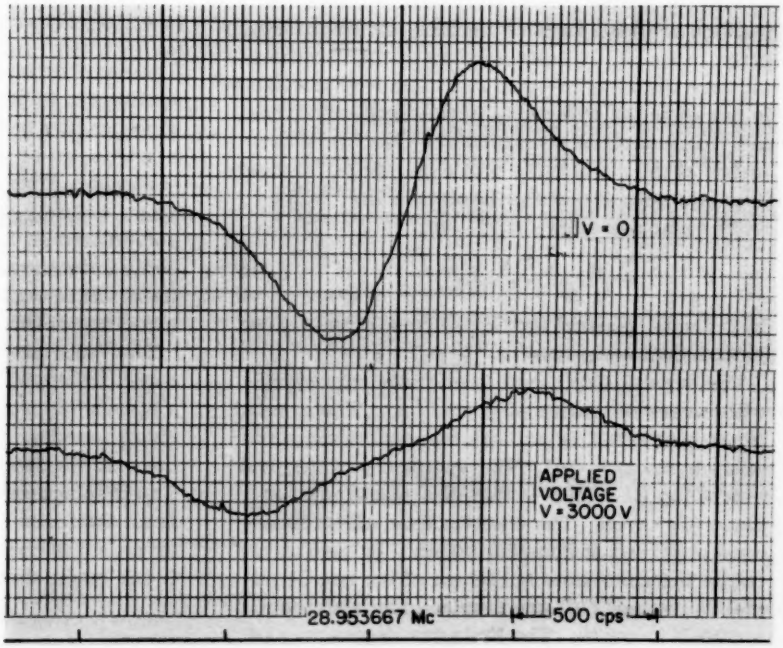

FIG. 1. The zero-field quadrupole resonance of Cl^{35} in polycrystalline $KClO_3$ at 77°K with and without applied electric field.

Table I. The observed second moment $\langle\Delta\nu^2\rangle$ and the width $\delta\nu$ between points of extreme slope of the Cl^{35} resonance as a function of the electric field strength E in polycrystalline $KClO_3$ and $NaClO_3$.

	E in kv/cm	$\langle\Delta\nu^2\rangle$ in cps^2	$\delta\nu$ in cps
$KClO_3$	0	65 000	480
	7.32	91 000	530
	14.6	137 000	990
$NaClO_3$	0	105 000	610
	7.32	117 000	690
	12.2	131 000	785
	17.1	···	905
	18.3	151 000	···

gradient components is then given by

$$e(\Delta q)_{ij} = \sum_{k=x,y,z} R_{ijk}E_k + \sum_{l,m=x,y,z}\sum S_{ijlm}e_{lm}. \quad (1)$$

The effect of variation with strain described by a fourth order tensor S was introduced earlier.[6,7] In piezoelectric crystals the application of an electric field produces a strain

$$e_{lm} = \sum_k d_{klm}E_k. \quad (2)$$

The interest here is clearly in the new physical effect of an electric field at constant strain. The symmetry properties of third and fourth order tensors are well known.[8] In fact, the relationship given in Eq. (1) is quite similar to the relations between the electro-optic and elasto-optic effects.[9] In our case the symmetry at the location of the individual nucleus counts rather than the symmetry of the crystalline unit cell. Since the electrostatic potential obeys Laplace's law, some trace relations exist,

$$\sum_i R_{iik} = \sum_i S_{iilm} = 0. \quad (3)$$

In the most general (triclinic) case R has fifteen independent constants.

The crystal $KClO_3$ has monoclinic symmetry with inversion center (C_{2h} or $2/m$). The crystal is not piezoelectric and has two equivalent molecules in the unit cell. The symmetry at the position of the Cl nuclei is that of a single mirror plane (C_s or m). The electric field effect is indeed observed at constant strain. In each crystallite the zero-field splittings of the two Cl nuclei in the unit cell are displaced by equal and opposite amounts. The Kramers degeneracy of the nuclear spin levels is <u>not</u> lifted. The effect has nothing to do with the existence of a nuclear dipole moment.[10,11] From a single observation of the variation of zero-field splitting, the eight independent components of the R tensor in the C_s symmetry can clearly not be determined. With a single crystal one could measure the variation in the zero-field splitting with the applied electric field in two directions within the plane of symmetry. This would still give only two components. The other components can in principle be determined by two methods which will be described below.

The crystal symmetry of $NaClO_3$ is cubic (23 or T). The symmetry at the position of the four Cl nuclei in the unit cell is trigonal (3 or C_3). The crystal is piezoelectric. It can, however, be estimated from the known piezoelectric constant and the known effect of hydrostatic compression on the quadrupole splitting[12] that the observed effect is mostly due to the first term on the right-hand side of Eq. (1). The first order change in the zero-field splitting ν_0 for this case of axial symmetry is thus given by

$$\Delta\nu/\nu_0 = (\Delta q_{zz}/q_0) = R_{zzz}E_z/q_0, \quad (4)$$

where the z axis is taken at each Cl nucleus pointing to the nearest Na nucleus. The increase in second moment in the powder is

$$\langle\Delta\nu^2\rangle_{el} = \tfrac{1}{3}R_{zzz}^2\langle E_0^2\rangle\nu_0^2/q_0^2. \quad (5)$$

The same formula may be used in a good approximation for $KClO_3$, since the deviations from axial symmetry in that case are quite small. This is borne out by the small value of the asymmetry parameter,[13] $\eta = 0.007$. There can be little doubt that a single crystal of $KClO_3$ would show a resolved doublet for the two Cl nuclei, which become nonequivalent on application of an electric field. This would throw further light on the structure of this crystal.[13]

The value of $|R_{zzz}|$ and $|\Delta q_{zz}|$ derived from experiment with Eqs. (4) and (5) agrees well with a simple theoretical estimate based on a point charge model. The electric field displaces the nearest alkali ion with respect to the Cl nucleus. The displacement Δr can be estimated either from the force constants of the ionic crystals or from the contribution of ionic displacements to the static dielectric constant ϵ_{dc},

$$\Delta r = (\epsilon_{dc} - n^2)E/4\pi Ne_{eff},$$

where N is the number of positive ions per unit volume with effective charge e_{eff} and n is the optical index of refraction. The change in quadrupole coupling is in order of magnitude given by

$$e\Delta q_{zz} = 6(1-\gamma_\infty)e_{\text{eff}}r^{-4}\Delta r,$$

or

$$R_{zzz} = 6(1-\gamma_\infty)(\epsilon_{\text{dc}}-n^2)(4\pi N r^4)^{-1}, \qquad (6)$$

where $1-\gamma_\infty$ is the Sternheimer factor, and r the anion-cation distance.

This oversimplified model should, of course, be improved in several ways, but it gives the observed value $|R_{zzz}| = 2.1\times10^9$ cm^{-1} with $1-\gamma_\infty = 35$. Its purpose is merely to illustrate the physical origin of the observed R tensor, which is closely related to the third derivatives of the electrostatic potential.

It would appear that only one constant, R_{zzz}, can be measured in the case of axial symmetry, both in the powder and in a single crystal. This would leave four other independent constants of the R tensor for C_3 symmetry in $NaClO_3$ undetermined. They relate to off-diagonal elements in the electric quadrupole interaction. If, however, an external magnetic field is applied to a single crystal at an angle with the axis of symmetry of sufficient strength to scramble the nuclear spin states so that the m_I's are poor quantum numbers, the various resonant frequencies between the four nuclear spin states will vary linearly with applied electric field components in the x and y direction. In principle, all components of R may be determined from such measurements.

It is perhaps of more interest to utilize the existence of off-diagonal elements proportional to the applied electric field for the induction of nuclear spin transitions by a radio-frequency electric field. The transition probabilities are proportional to the square of the electric field strength and can readily be calculated from Eq. (1) and the known matrix elements of the nuclear quadrupole operator. The components Δq_{xz} and Δq_{yz} will be connected with $\Delta m_I = \pm1$ transitions and $\Delta q_{xx} - \Delta q_{yy}$ with $\Delta m_I = \pm2$ transitions. The resonant absorption may be described by an effective nuclear dielectric susceptibility, $\epsilon''/4\pi$. The coupling strengths of the nuclear spin to applied electric and magnetic fields may be compared with each other. The last column in Table II has only order-of-magnitude significance since differences in magnitude between the nonvanishing components of R and between the nuclear spin operator matrix elements have been ignored. In principle, accurate measurements of the effective nuclear dielectric susceptibility tensors would determine the other components of R. Such experiments bear, of course, a close resemblance to acoustically induced resonances.[7] The electrical resonances at constant strain have the advantage that acoustical propagation effects are absent. Electric radio-frequency fields of the required magnitude and uniformity can readily be obtained.

For the heavier elements the coupling to the electric field becomes large enough that it may be detectable directly as a decrease in Q of a capacitance. An electric field of 3 kv/cm applied at the Cl^{35} resonant frequency in $KClO_3$ at room temperature would saturate that spin resonance. Double-resonance experiments are feasible, in which, e.g., an electric radio-frequency field saturates a $|\Delta m| = 2$ transition and a magnetic radio-frequency field monitors a $|\Delta m| = 1$ transition. Electric 90° and 180° pulses are possible. Numerous other electric variations of magnetic resonance experiments suggest themselves.

The phenomenological description given here

Table II. Comparison of electric and magnetic nuclear spin coupling.

Nucleus	Crystal	Quadrupole splitting ν_0 in Mc/sec	Stark shift for 10^4 v/cm along axis of symmetry $\Delta\nu$ in cps	ΔH in gauss	$\epsilon''/4\pi\chi''$
Na^{23}	$NaClO_3$	0.89	50[a]	0.044[a]	2×10^{-6} [a]
Cl^{35}	$NaClO_3$	30.6	250[b]	0.6	3.3×10^{-4} [a]
Br^{81}	$NaBrO_3$	150	2500[c]	0.23	5×10^{-3} [a]

[a] Theoretical estimate.
[b] From data of Table I and Eqs. (4) and (5).
[c] Experimental value from reference 2.

is quite general and can readily be applied to other situations. Consider, e.g., integral spins in axial symmetry. The levels m_I and $-m_I$ are degenerate. An applied electric field off axis will lift the degeneracy of the levels $m_I = \pm 1$ in first order. This is a true linear Stark splitting of a degenerate level.

An interesting situation occurs if the nucleus occupies a cubic site without inversion symmetry. In the III-V compounds with ZnS structure the nucleus occupies a site with $T_d = \bar{4}\,3m$ symmetry. There is no quadrupole interaction and an external magnetic field will give $2I+1$ equally spaced levels with one resonant frequency. If an electric field is applied—some III-V compounds, such as GaAs, can be obtained of sufficiently high resistivity that fields of 10 kv/cm or more can be maintained—the nuclei are displaced from their positions of cubic symmetry. A first order quadrupole splitting or broadening proportional to E should result, which can readily be calculated for arbitrary orientations of $\vec{E}$ and $\vec{H}_0$. The R tensor is characterized by one constant in this case.

Similar effects in electron spin resonance can be expected, if a paramagnetic ion occupies a site without inversion symmetry. Odd terms in the crystalline field potential will give rise to changes in the constants of the spin Hamiltonian on displacement of the ion by an applied electric field. Linear variations in optical absorption frequencies of transition metal ions may also occur.[14] The ratio of the displacement of the resonant line for a given applied electric field to the linewidth is generally less favorable in these cases.

---

*Research was supported by the U. S. Joint Services.

[1]N. Bloembergen, Science 133, 1363 (1961).

[2]T. Kushida and K. Saiki, this issue [Phys. Rev. Letters 7, 9 (1961)]. We thank Dr. Kushida for communicating his results before publication and for a stimulating discussion.

[3]J. Jeener, Rev. Sci. Instr. 32, 27 (1961).

[4]C. J. F. Böttcher, Theory of Electric Polarization (Elsevier Publishing Company, Amsterdam, 1952), p. 415.

[5]D. A. Jennings and W. H. Tanttila, Rev. Sci. Instr. 30, 137 (1959).

[6]R. G. Shulman, B. J. Wyluda, and P. W. Anderson, Phys. Rev. 107, 953 (1957).

[7]E. F. Taylor and N. Bloembergen, Phys. Rev. 113, 431 (1959).

[8]W. Voigt, Lehrbuch der Kristallphysik (B. G. Teubner, Leipzig, 1910).

[9]G. Szivessy, Handbuch der Physik, edited by S. Flügge (Spinger-Verlag, Berlin, 1929), Vol. 21, Chap. 19.

[10]J. H. Smith, E. M. Purcell, and N. F. Ramsey, Phys. Rev. 108, 120 (1957).

[11]M. E. Browne, Phys. Rev. 121, 1699 (1961).

[12]H. S. Gutowski and G. A. Williams, Phys. Rev. 105, 464 (1957).

[13]H. Zeldes and R. Livingston, J. Chem. Phys. 26, 1102 (1957).

[14]W. Kaiser, S. Sugano, and D. L. Wood, Phys. Rev. Letters 6, 605 (1961).

DIRECT EXPERIMENTAL MEASUREMENT OF THE MAGNETIC FIELD DEPENDENCE OF THE SUPERCONDUCTING ENERGY GAP OF ALUMINUM

D. H. Douglass, Jr.

Lincoln Laboratory,* Massachusetts Institute of Technology, Lexington, Massachusetts

(Received June 7, 1961)

This Letter reports experimental measurements of the field dependence of the superconducting energy gap of aluminum. The energy gap was measured directly by using the electron tunnelling technique.[1,2] The magnetic field was longitudinal and the reference superconductor was lead. In Fig. 1 the normalized energy gap vs reduced magnetic field is shown for two films of thickness 3000 A and 4000 A. It should be noticed that for the 3000A film the energy gap goes smoothly to zero as the critical field is approached. It is described quite well by the equation $[\epsilon(H)/\epsilon(0)]^2 = 1 - (H/H_c)^2$. This behavior implies a second order phase transition. Measurements on two other films of thickness 500 A and 2000 A gave similar results. Also, these results were independent of temperature over the range available ($0.75 < T/T_c < 1.00$). For the 4000A film an entirely different behavior is observed. The gap initially drops less rapidly with field than in the previous case, and as the critical field is approached the energy gap drops very abruptly from a finite value to zero; this abrupt change usually occurs within less than 1% of the critical field. The value of the gap just prior to this abrupt drop will be called the critical gap. The critical gap of the 4000A film was

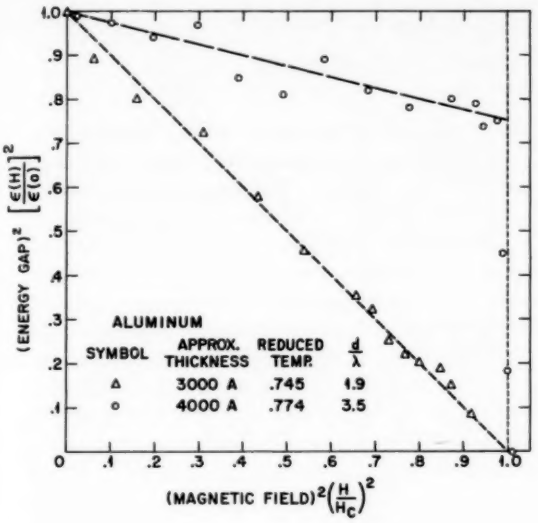

FIG. 1. Energy gap of aluminum vs magnetic field for films of thickness 3000 A and 4000 A. Two other films of thickness 500 A and 2000 A behaved similarly to the 3000A film. The dashed curves are the best straight lines through the data points.

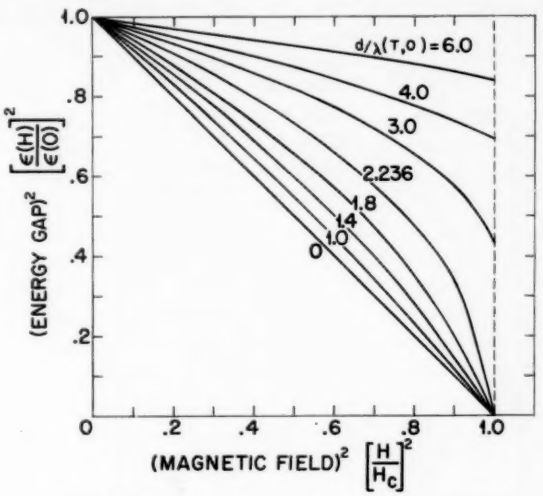

FIG. 2. Energy gap vs magnetic field according to the Ginzburg-Landau-Gor'kov theory for various ratios of thickness to penetration depth.

found to be a function of temperature.

Douglass[3] has pointed out that the Ginzburg-Landau[4] theory with Gor'kov's[5] addition could be used to explain the field dependence of the energy gap. Figure 2 shows the predictions of the theory which were obtained by solving Eqs. (1) and (2) of reference 3. According to the theory, the nature of the curve is a function only of the ratio of the thickness, d, to the penetration depth, λ. For small values of d/λ the curves obey the equation $[\epsilon(H)/\epsilon(0)]^2 = 1 - (H/H_C)^2$. As d/λ becomes larger the curves bow upward with the energy gap continuing to go smoothly to zero at the critical field (i.e., the critical gap remains equal to zero). For $d/\lambda > \sqrt{5}$ the critical gap assumes a finite value, indicating that the phase transition has become first order. Thus, for $d/\lambda < \sqrt{5}$ the theory predicts a critical gap of zero and a second order phase transition, and for $d/\lambda > \sqrt{5}$ it predicts a finite critical gap and a first order phase transition. The experimental data of Fig. 1 show that these two types of predicted behavior are in fact observed, although the predicted bowing of the curves does not seem to occur. Values of d/λ for the various films were calculated[6] from the measured critical fields using the Ginzburg-Landau theory. For a given thickness one can vary d/λ over a range of values by changing the temperature since λ is temperature dependent. The largest attainable value of d/λ is limited by the value of λ at low temperatures, and the smallest value of d/λ is determined by how close one can get to the critical temperature and still have signals big enough to measure. Values of d/λ between 2.42 and 3.62 for the 4000A film were obtained by varying the reduced temperature between 0.749 and 0.965.

Experimental measurements of the critical gap are shown along with the theoretical curve[3] in Fig. 3. Measurements were made on four different films covering a range of d/λ from 0.10 to 3.52. It is seen that the data agree very well with the theory when d/λ is less than 2.8. The transition from first to second order is not inconsistent with $d/\lambda = \sqrt{5}$; the data show that it occurs for a d/λ between 1.9 and 2.4. For d/λ greater than 2.8 the value of the critical gap deviates from the theoretical curve.

There are two limitations on the Ginzburg-Landau-Gor'kov theory. The first is that it is true only in the local limit. This means that the penetration depth λ must be larger than the coherence length ξ, which certainly is not true in the bulk state of aluminum where $\lambda(T=0) \cong 500$ A and $\xi_0 \cong 15\,000$ A. However, one would expect that for a thin evaporated film the coherence length would be limited by the size of the crystallites. Thus the condition of locality would be

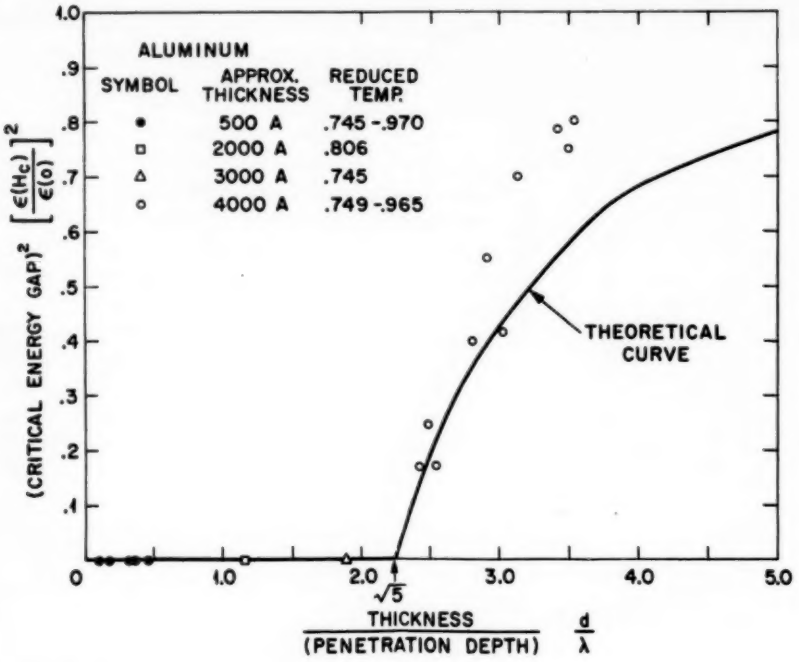

FIG. 3. Superconducting critical gap of aluminum vs ratio of thickness to penetration depth.

$\lambda > d$, which is much easier to satisfy, and nonlocal effects will start to become important when d becomes comparable to λ. Therefore, it is not surprising that deviations from the theory occur at $d/\lambda \approx 3$. For a metal for which the bulk penetration depth is greater than the bulk coherence length, the theory should be good for all d/λ. The second limitation concerns the fact that Gor'kov derived the Ginzburg-Landau equations from the microscopic theory under the condition that the energy gap was small compared to its value at zero temperature and zero field. The theory is therefore valid near the transition temperature where the gap is small. For thin films it can be made valid even at $T = 0$ by turning on a magnetic field.

In summary, we have measured the magnetic field dependence of the superconducting energy gap of aluminum films as a function of the ratio of the film thickness to the penetration depth. The critical gap was found to be zero for values of this ratio less than 1.9 and equal to a finite value for values greater than 2.4. The agreement between these experiments and the Ginzburg-Landau-Gor'kov theory is very good.

The author is grateful to R. Tweed for the fabrication of the films and to Dr. R. Meservey, who assisted in some of the data taking. He is also grateful for helpful discussions with Dr. E. Maxwell and Dr. C. E. Chase.

Note added in proof. Morris and Tinkham,[7] from thermal conductivity measurements, have also determined the field dependence of the energy gap in thin films. They come to conclusions similar to those presented here.

---

*Operated with support from the U. S. Army, Navy, and Air Force.

[1]I. Giaever, Phys. Rev. Letters 5, 464 (1960).

[2]J. Nicol, S. Shapiro, and P. H. Smith, Phys. Rev. Letters 5, 461 (1960).

[3]D. H. Douglass, Jr., Phys. Rev. Letters 6, 346 (1961).

[4]V. L. Ginzburg and L. D. Landau, J. Exptl. Theoret. Phys. (U.S.S.R.) 20, 1064 (1950).

[5]L. P. Gor'kov, J. Exptl. Theoret. Phys. (U.S.S.R.) 36, 1918 (1959) [translation: Soviet Phys.—JETP 9, 1364 (1959)].

[6]There are as yet no data relating d/λ to d for aluminum. It might be argued that using the Ginzburg-Landau theory to calculate d/λ from the critical field amounts only to a self-consistency check; however, estimates of d/λ using the approximate thickness and the bulk penetration depth, modified by size effects according to M. Tinkham [Phys. Rev. 110, 26 (1958)], give values which do not differ by more than 20-30% from those quoted here.

[7]D. E. Morris and M. Tinkham, Phys. Rev. Letters 6, 600 (1961).

PARAMAGNETIC RESONANCE DETECTION OF LUMINESCENT CENTERS AND TRAPS IN SELF-ACTIVATED ZnS PHOSPHORS

Paul H. Kasai and Yoshiro Otomo
Hitachi Central Research Laboratory, Kokubunji, Tokyo, Japan
(Received May 22, 1961)

The atomic nature of the luminescent center in self-activated ZnS phosphors has been the subject of many papers.[1-4] Kröger and Vink[1] have proposed that the self-activated centers are Zn^{++} ion vacancies that have lost one electron from their nearest surrounding S^{--} ions. Magnetic susceptibility measurements by Bowers and Melamed,[2] however, revealed that the self-activated center is diamagnetic, whereas the model proposed by Kröger and Vink should be paramagnetic. Prener and Williams[3] then suggested a model in which the centers in question are Zn^{++} ion vacancies with one of their charge-compensating ions (Cl^-, Br^-, I^-, Al^{+++}, or Ga^{+++}) associated at the nearest possible sites in the ZnS lattice. More recently Prener and Weil[4] supported the latter model by showing experimentally that the emission peak of the self-activated luminescence depends on whether a group III-*B* or group VII-*B* element is used as a coactivator. The existence of various traps for excited electrons or holes in luminescent ZnS phosphors including the self-activated type are also well known,[5] though here again the problems concerning the exact nature of some of these traps are still unsettled. If the self-activated ZnS phosphor is truly diamagnetic in its unexcited state, then the presence of such traps implies that the phosphor should become paramagnetic when enough electrons are transferred from the luminescent centers into these traps as is often done in thermoluminescence experiments. The following is the preliminary report of our electron paramagnetic resonance (EPR) detection of such excited states frozen at the liquid nitrogen temperature.

The polycrystalline samples of self-activated ZnS phosphors were prepared by firing the luminescent grade ZnS powder using various alkali halides (NaCl, NaBr, KCl, and KBr) as flux at 800°C for 3 hours. A comparatively low firing temperature was employed in order to ensure the formation of cubic crystals. The x-ray analysis did prove that they were all cubic, and all of them exhibit a single emission band peaking around 4640 A characteristic of the self-activated emission.

In parallel with the result of Bowers and Melamed, none of these samples give an EPR signal in the dark, either at room temperature or at 77°K, except six equally spaced weak lines due to a trace of Mn^{++} impurity. At room temperature, simultaneous illumination of the sample with 3650A ultraviolet radiation produced no change in the observed spectra. At liquid nitrogen temperature, however, the simultaneous ultraviolet illumination gave rise to two additional signals *A* and *B* in every sample. Figure 1 shows such spectra obtained with ZnS(NaCl) and ZnS(NaBr), respectively. Changing the cation of the flux from Na^+ to K^+ has no effect upon the spectra.

The shape of the signal *B* is more or less symmetric, and is little affected when the halide ion in the flux is changed. The *g* value of the signal *B* is 1.883 ± 0.001. The fact that its *g* value is less than 2 implies that the signal *B* is associated with un-ionized donors, namely filled traps.[6]

The shape of the signal *A* is just what one would expect for a polycrystalline sample having an anisotropic *g* value.[7] Also, as can be seen from the figure, when Cl^- in the flux is replaced by Br^-, the apparent linewidth becomes much broader. In either case the *g* values observed on the signal *A* are

$$g_\perp = 2.052 \pm 0.001,$$

$$g_\parallel = 2.027 \pm 0.005.$$

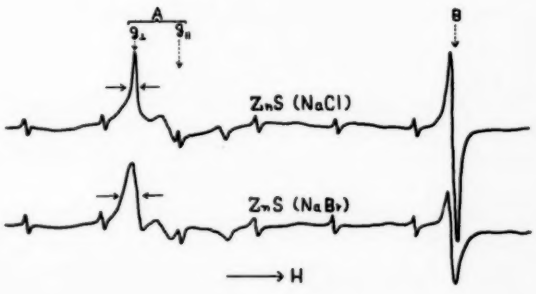

FIG. 1. EPR spectra of self-activated ZnS phosphors under ultraviolet illumination at 77°K. Six equally spaced weak signals are due to Mn^{++} ion impurity, each spacing being approximately 68 gauss.

It should be noted that the mean g value is greater than the free spin value, implying that the signal A is caused by a hole, an empty acceptor.

Both signals A and B are found to decay when the illumination is stopped. The rate of the decay is quite slow at 77°K except for the first few minutes immediately after stopping the excitation. Approximately half of the original intensity can be still detected after 5 hours, so long as the sample is kept in the dark at 77°K. The rapid initial decay may be what is responsible for the glow peak observed near liquid nitrogen temperature in the thermoluminescence experiments.[5,8,9] The subsequent slow but steady decay is probably due to the tunneling process discussed by Hoogenstraaten.[5]

Among many defects which can act as electron traps in the ZnS phosphors, the Co^{++} ion is known to provide one of the deepest traps.[5] Consequently if our previously stated analysis concerning the nature of the signals A and B is correct, the introduction of Co^{++} ions into these phosphors should result in a strong enhancement of the signal A and weakening of the signal B. This was indeed found to be the case. Introduction of 10^{-6} (mole ratio) $CoCl_2$ increased the intensity of the signal A by a factor of five while making the signal B appear only as a trace. Figure 2 shows the spectrum obtained with ZnS(KCl) containing 10^{-5} Co^{++}. A strong broad resonance at the left is due to Co^{++} ions. The g value of this Co^{++} resonance is 2.248 ± 0.005.[10] In Fig. 1 one also notices a weak negative dip near the $g = 2.00$ position, the center of the six Mn^{++} hyperfine components. This signal, however, cannot be incorporated into the signal A, since it does not grow upon the introduction of Co^{++} ions. The nature of this signal is still unknown.

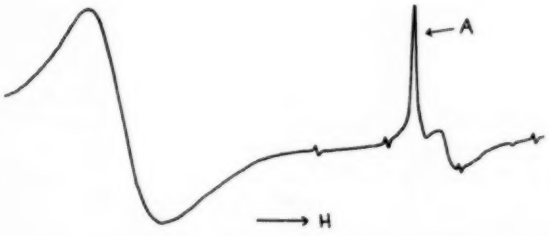

FIG. 2. EPR spectrum obtained with ZnS:10^{-5}Co(KCl) under ultraviolet illumination at 77°K. A strong broad resonance at the left is due to the Co^{++} ion. Note the enhancement on signal A. The amplifier gain used for this record was about 1/3 of that used for the records in Fig. 1.

If the defect responsible for the signal A is a simple Zn^{++} ion vacancy surrounded by four S^{--} ions at the tetrahedral corners, the observed anisotropy in the g value and the dependency of the line shape upon the halide ion in the flux are both difficult to explain. We, therefore, believe that the signal A is caused by the defect proposed by Prener and Williams.[3] The Zn^{++} ion vacancy surrounded by three S^{--} ions and one halide ion at the tetrahedral corners could well account for the above-mentioned features of this signal. Also since there is no significant change in the g value when Cl^- in the flux is replaced by Br^-, we must attribute the observed difference in the line shape to the difference in the nuclear magnetic moments of the respective halogen nuclei. A careful study of the spectra revealed that the ratio of the apparent linewidth of the signal A (the width shown by the arrows in Fig. 1) of ZnS(NaCl) to that of ZnS(NaBr) is 1:2.8, in close agreement with the ratio of the average magnetic moments of the respective halogen nuclei. The nature of the defect responsible for the signal B is less certain. The chloride flux always produces more of this signal than the bromide, though there is no significant change in the line shape, nor in the g value. The sulfur vacancies produced by some chemical reaction involving the alkali halide flux are probably responsible for this signal.

The EPR spectrometer used for this work is a Varian 100-kc spectrometer, model V-4500, and the frequency of the microwave is about 9.2 kMc/sec.

A more detailed and fuller account of this work will be published in the future together with the work on a single crystal which is now in progress.

[1]F. A. Kröger and H. J. Vink, J. Chem. Phys. 22, 250 (1954).

[2]R. Bowers and N. T. Melamed, Phys. Rev. 99, 1781 (1955).

[3]J. S. Prener and F. E. Williams, J. Chem. Phys. 25, 361 (1956).

[4]J. S. Prener and D. J. Weil, J. Electrochem. Soc. 106, 409 (1959).

[5]W. Hoogenstraaten, Philips Research Repts. 13, 515 (1958).

[6]See also J. Lambe and C. Kikuchi, J. Phys. Chem. Solids 8, 492 (1959).

[7]J. W. Searl, R. C. Smith, and S. J. Wyard, Proc. Phys. Soc. (London) 74, 491 (1959).

[8]N. Riehl and H. Ortmann, Z. Naturforsch. 10a, 896 (1955).

[9]H. Arbell and A. Halperin, Phys. Rev. 117, 45 (1960).

[10]See also F. S. Ham, G. W. Ludwig, G. D. Watkins, and H. H. Woodbury, Phys. Rev. Letters 5, 468 (1960).

MAGNETIC SHIELDING CONSTANTS IN HETEROPOLAR DIATOMIC MOLECULES

C. William Kern and William N. Lipscomb
Department of Chemistry, Harvard University, Cambridge, Massachusetts
(Received June 5, 1961)

The general theory of magnetic shielding of nuclei in molecules, first developed by Ramsey[1] using perturbation theory, showed that the screening effect at the nucleus was due to motions of molecular electrons. More recent variational and atomic theories[2] of chemical shielding in simple molecules give results in agreement with Ramsey's conclusions. As generally applied, the perturbation approach requires a knowledge of all the excited states of the molecule, including the continuum.[3] However, we show here that when a suitable choice is made for the vector potential, the excited state portion of Ramsey's formula vanishes.[4] The magnetic shielding is then reduced to matrix elements over the ground-state wave function.

When a diatomic molecule, AB, in a $^1\Sigma$ ground-state configuration and containing $2n$ electrons is placed in a homogeneous magnetic field, $\vec{H}$, the Hamiltonian for the electronic system can be written as[5]

$$\mathcal{H} = \tfrac{1}{2}\sum_{\mu=1}^{2n}\left[i^{-1}\nabla_\mu + \frac{1}{c}\left(\tfrac{1}{2}\vec{H}\times(\vec{r}_{A\mu} - b\vec{R}) + \frac{\vec{u}_A\times\vec{r}_{A\mu}}{r_{A\mu}^3}\right)\right]^2 + V,$$

where $\vec{R}$ is the vector pointing from nucleus A to B, b is a dimensionless constant to be determined, and magnetic effects of nucleus B, molecular rotations, and electron spin have been neglected.

Following Ramsey,[1] we show that the expression for the magnetic shielding constant of nucleus A, averaged over all orientations of the molecule with respect to the applied field, becomes

$$\sigma_A = \frac{1}{3c^2}\langle 0|\sum_{\mu=1}^{2n} 1/r_{A\mu}|0\rangle - \frac{bR}{3c^2}\langle 0|\sum_{\mu=1}^{2n} z_{A\mu}/r_{A\mu}^3|0\rangle - \frac{1}{3c^2}\sum_{n'=1}^{\infty}(E_{n'}-E_0)^{-1}$$

$$\times\Big[\langle 0|\sum_{\mu=1}^{2n} M_{xA\mu}/r_{A\mu}^3|n\rangle\langle n'|\sum_{\mu=1}^{2n} M_{xA\mu}|0\rangle + \langle 0|\sum_{\mu=1}^{2n} M_{xA\mu}|n'\rangle\langle n'|\sum_{\mu=1}^{2n} M_{xA\mu}/r_{A\mu}^3|0\rangle$$

$$+ bR\langle 0|\sum_{\mu=1}^{2n} M_{xA\mu}/r_{A\mu}^3|n'\rangle\langle n'|\sum_{\mu=1}^{2n} p_{y\mu}|0\rangle + bR\langle 0|\sum_{\mu=1}^{2n} p_{y\mu}|n'\rangle\langle n'|\sum_{\mu=1}^{2n} M_{xA\mu}/r_{A\mu}^3|0\rangle\Big],$$

where $M_{xA\mu}$ and $p_{y\mu}$ are the x and y components of the angular and linear momentum of electron μ. We have assumed right- and left-handed coordinate systems on nuclei A and B, respectively. Using the well known closure property,[6] the choice of b which renders the second-order perturbation sum zero is

$$b = -\frac{\langle\Delta E_1\rangle_{av}}{\langle\Delta E_2\rangle_{av}}\frac{\langle 0|\sum M_{xA\mu}M_{xA\nu}/r_{A\mu}^3|0\rangle}{R\langle 0|\sum M_{xA\mu}p_{y\nu}/r_{A\mu}^3|0\rangle} \cong -\frac{\langle 0|\sum M_{xA\mu}M_{xA\nu}/r_{A\mu}^3|0\rangle}{R\langle 0|\sum M_{xA\mu}p_{y\nu}/r_{A\mu}^3|0\rangle},$$

where $\langle\Delta E_1\rangle_{av}$ and $\langle\Delta E_2\rangle_{av}$ are average excitation energies corresponding to the pairs of operators $(M_{xA\mu}/r_{A\mu}^3, M_{xA\mu})$ and $(M_{xA\mu}/r_{A\mu}^3, p_{y\mu})$, respectively. We assumed $\langle\Delta E_1\rangle_{av} = \langle\Delta E_2\rangle_{av}$ since, for heteropolar diatomic molecules, all operators in the excited state sum belong to the same irreducible

Table I. Magnetic shielding in two heteronuclear diatomic molecules.[a]

Molecule	Calculated diamagnetic shielding of H	Experimental diamagnetic shielding of H	Calculated paramagnetic shielding of H	Experimental paramagnetic shielding[b] of H
LiH	39.52	...	-14.95	-13.8 ±0.5[c]
HF	110.67[d]	110.9[e]	-87.30	-79.6 ±0.5[f]

[a] All results expressed in parts per million.

[b] Calculated from spin-rotation interaction constants.[1]

[c] $C_H = +8 \pm 1$ kc/sec, L. Wharton, L. P. Gold, and W. Klemperer (private communication).

[d] J. Kolker and M. Karplus obtained 110.68 ppm using more exact values for the molecular integrals. These authors are also engaged in calculating the paramagnetic shielding in these molecules with a multiterm variation function (private communication).

[e] J. N. Pinkerton and C. H. Anderson, Bull. Am. Phys. Soc. 6, 281 (1961).

[f] $C_H = +71 \pm 3$ kc/sec, M. R. Baker, H. M. Nelson, J. A. Leavitt, and N. F. Ramsey, Phys. Rev. 121, 807 (1961).

representation of $C_{\infty v}$, i.e., the same excited states contribute to each term. Hence, we find for the magnetic screening constant[7]

$$\sigma_A = \frac{1}{3c^2}\langle 0|\sum 1/r_{A\mu}|0\rangle + \frac{1}{3c^2}\frac{\langle 0|\sum M_{xA\mu} M_{xA\nu}/r_{A\mu}^3|0\rangle\langle 0|\sum z_{A\mu}/r_{A\mu}^3|0\rangle}{\langle 0|\sum M_{xA\mu} p_{y\nu}/r_{A\mu}^3|0\rangle}. \quad (1)$$

We have evaluated the diamagnetic and paramagnetic shielding constants for the proton in LiH and HF from Eq. (1).[8] The results, given in Table I, are in reasonable agreement with experiment. Applications to the chemical shielding and diamagnetic susceptibility in other diatomic systems, including the anomalous proton and fluorine shielding in transition metal complexes, are in progress. Details of these calculations will be published later.

We are indebted to Mr. Russell M. Pitzer and Professor M. P. Barnett for much helpful discussion and assistance in evaluation of the integrals. The calculations were done in part at the Massachusetts Institute of Technology Computation Center. Acknowledgement is accorded the Office of Naval Research for financial aid to one of us (C.W.K.).

[1] N. F. Ramsey, Phys. Rev. 77, 567 (1950); 78, 699 (1950); 83, 540 (1951); 86, 243 (1952).

[2] For a summary, see J. G. Powles, Reports on Progess in Physics (The Physical Society, London, 1959), Vol. 22, p. 433.

[3] L. C. Snyder and R. G. Parr, J. Chem. Phys. 34, 837 (1961).

[4] A variational method for eliminating the excited state sum in the expression for the diamagnetic susceptibility has been proposed by T. K. Rebane, J. Exptl. Theoret. Phys. (U.S.S.R.) 38, 963 (1960) [translation: Soviet Phys. – JETP 11, 694 (1960)]. M. Baker has calculated the diamagnetic susceptibility of molecular hydrogen with this procedure and has proposed its extension to magnetic shielding (private communication).

[5] Hartree atomic units ($\hbar = 1$, $m = 1$, $e = 1$) are used throughout.

[6] L. Schiff, Quantum Mechanics (McGraw-Hill Book Company, New York, 1955). For limitations, see A. D. McLachlan, J. Chem. Phys. 32, 1263 (1960).

[7] K. Ito, J. Am. Chem. Soc. 80, 3502 (1958), has also cancelled average excitation energies but in a different manner. His method, which was shown later [Y. Kurita and K. Ito, J. Am. Chem. Soc. 82, 296 (1960)] to be equivalent to a variational calculation, amounts to placing the origin of the vector potential at the center of electronic charge and assuming the excited state sum is zero for that origin.

[8] Wave functions taken from B. J. Ransil, Revs. Modern Phys. 32, 245 (1960).

FIELD-SWEPT MASER OSCILLATION

James C. Kemp
Department of Physics, University of Oregon, Eugene, Oregon
(Received May 1, 1961)

Recently Singer and Wang[1] (SW) have put forth an analysis which purportedly describes the behavior of a very wide variety of maser oscillators. An experimental verification was offered, based on a pulsed maser oscillation waveform from the present writer's work.[2]

The purposes of the present note are as follows: (1) To show that our waveforms, on one of which SW based their Fig. 1, show large qualitative and quantitative discrepancies from their predicted radiation envelope structure. For this purpose we will first discuss their main Eq. (8) and show how its solution (SW Fig. 2) differs from our waveforms. Our reason for the discrepancies is that our oscillator was of the "field-swept" type, in which emission occurs as the Zeeman field value H_0 is swept through resonance, giving a radiation envelope determined largely by the H_0 sweep rate and showing a modulation due, we believe, to a mechanism unrelated to that invoked by SW. (2) To summarize our own analysis[2] of the oscillator behavior, which we feel conforms adequately with our waveforms. In particular our asymptotic form [Eq. (2) below] for relatively fast sweep and weak oscillation will be seen to agree quantitatively within experimental limits, and qualitatively in all details, with an appropriate sample (Fig. 3) from a series of oscillograms.[2] We hope this note will help explain waveforms seen in other paramagnetic maser oscillators involving H_0 sweep.

As for the nature of the SW solution, the nutation-angle substitution[3] $\theta = \int_0^t 2\hbar\mu H(t')dt'$ in their Eq. (8), with $pE \to \mu H$ and N_e constant, the relevant case, gives $\ddot{\theta} + \tau^{-1}\dot{\theta} + (\tau\tau_\gamma)^{-1}\sin\theta = 0$, the simple damped-pendulum equation, where $\tau = 2Q/\omega$ = cavity ringing time and τ_γ = radiation damping time.[4] This writer noted previously[3] (see also Yariv[5]) that even with $\theta(0) \sim \pi$ (initial inverted state), in the pertinent case the radiation amplitude $H = \gamma^{-1}\dot{\theta}$ is given adequately by $\exp(-t/\tau) \times \sin[t/(\tau\tau_\gamma)^{1/2}]$ after the first "cycle" or two. The resulting emission would have mean duration of order τ and would show roughly uniform 100% modulation with period of order $(\tau\tau_\gamma)^{1/2}/2\pi$. In our experiments[2] $\tau \cong 0.6\,\mu$sec. Our observed durations depended on the sweep rate, and ranged[2] from 7 μsec (fastest sweep) to 500 μsec (slowest sweep), with representative values 500, 15, and 90 μsec, respectively, for Figs. 1, 2,

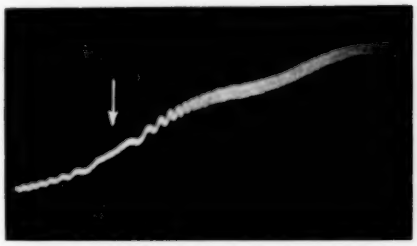

FIG. 1. Field-swept maser oscillation, displaying emission envelope $|H(t)|$. Slow sweep, $dH_0/dt = 800$ gauss/sec. $\beta \cong 0.001$; $\tau_\gamma \cong 0.1\,\mu$sec. Trace length 200 μsec. Fractional Zeeman energy release ~70%. Shown here is the rising portion of the envelope, which decays to the right. The thickness of the trace in the upper part is not noise but unresolved rapid modulation. The arrow is believed in the vicinity of passage through the line-center resonance ($t = 0$), though this point was not localized experimentally. Equation (2) of text is not applicable.

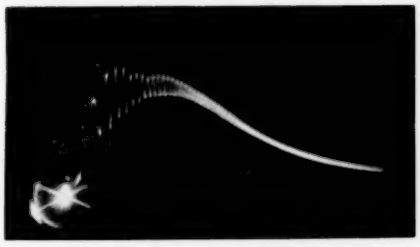

FIG. 2. Field-swept emission. $dH_0/dt = 2\times10^4$ gauss/sec. $\beta \cong 0.03$; $\tau_\gamma \cong 0.1\,\mu$sec. Trace length 30 μsec. Owing to the fast sweep, in spite of about 50% Zeeman energy release the modulation pattern is surprisingly like that of Eq. (2) except for average shallowness. Period of fifth modulation cycle $T_5 = 1.2\,\mu$sec (theor) = 0.8 μsec (exp).

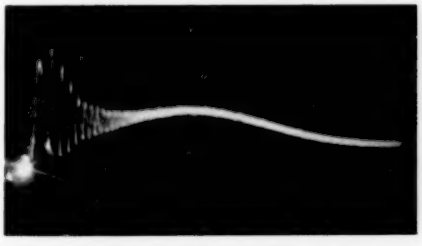

FIG. 3. Field-swept emission. $dH_0/dt = 4\times10^3$ gauss/sec. $\beta \cong 0.03$; $\tau_\gamma \cong 0.6\,\mu$sec. Trace length 200 μsec. Energy release ~30%. $T_5 = 2.8\,\mu$sec (theor) = 4.0 μsec (exp). Equation (2) well describes this plus seven other oscillograms in reference 2, with moderate to rapid sweep and not too strong oscillation.

and 3 shown in this note. Our waveforms show, rather than uniform 100% modulation, a modulation with frequency increasing indefinitely with time, after sweep through resonance, with a percent depth that depends strikingly on the sweep rate.

The possibility of observing two-level paramagnetic maser oscillation showing the pendulum-like behavior[6] expected from a static-H_0 analysis[1,3] was investigated by the writer.[2] We concluded that, when one induces oscillation by the common procedure of sweeping the field H_0 into or through resonance, at least in our apparatus it was impossible to establish oscillation conditions "suddenly" enough to allow emission to occur with essentially static parameters (the field H_0). Emission with H_0 varying in time linearly through resonance was then studied systematically, and was the subject of our work,[2] which we now summarize.

Our theoretical treatment[2] of the field-swept case starts with the coupling equation between a complex radiation field amplitude H and a complex transverse magnetization M. For sweep through resonance rapid enough to allow only a small fractional Zeeman energy release, such that $M_z \cong -M_0$ holds, the spin-dynamic equations are soluble explicitly for arbitrary $H(t)$ and $\Delta H_0(t) = H_0(t) - \omega/\gamma$. We choose $\Delta H_0 = \gamma^{-1}\alpha t$, where α is a constant sweep rate. We assume a Lorentz line of width $(T_2^*)^{-1}$ and, for convenience,[7] that $T_2^* \cong \tau$. One gets

$$\frac{d^2H}{dt^2} + \left(\frac{2}{\tau} - i\alpha t\right)\frac{dH}{dt} + \frac{1}{\tau}\left(\frac{1}{\tau} - \frac{1}{\tau_\gamma} - i\alpha t\right)H = 0, \qquad (1)$$

which is readily transformable to Weber's equation.[8] The pertinent solution, in terms of a Weber's function of imaginary order, is

$$H = K \exp[(i\alpha t^2/4 - t/\tau)D_{i/\beta}[-(1+i)(\alpha/2)^{1/2}t],$$

with K = const. From asymptotic forms[2,8] we find, for moderate to rapid sweep,

$$|H(t)| \cong A(t)\left[1 + \frac{1}{\beta^{1/2}\alpha^{1/2}t}\sin(\tfrac{1}{2}\alpha t^2 + \phi)\right], \qquad (2)$$

where ϕ varies slowly and $\beta = \alpha\tau\tau_\gamma$ is a dimensionless sweep rate. This form described the radiation envelope for $\beta \gtrsim 1/8\pi \cong 0.04$ and $t \gtrsim (2\pi/\alpha)^{1/2}$. $|H(t)|$ rises monotonically during the interval about passage through resonance ($t = 0$). $A(t)$, giving the gross shape, rises to simple maximum at roughly $t_1 = \beta^{-1}(2\tau_\gamma/\tau)^{1/3}\tau$, and then decays, asymptotically like $\exp(t/\tau - 1/\beta^2\alpha t^2)$. The sine term gives an amplitude modulation, with fractional depth about 100% (for $\beta \sim 1/8\pi$) initially, but decreasing in percentage as $1/t$, and increasing indefinitely in frequency with t.

The modulation mechanism described by (1) and (2) inherently involves the time-varying H_0, which continually tends to throw the magnetization into the wrong phase, with respect to the radiation field, for oscillation buildup. Modulation due to this mechanism should vanish for vanishingly slow sweep.[9]

Figures 1-3 are from the writer's experimental field-swept oscillator,[2] and display $|H(t)|$. Relevant measured parameters were: $\tau \cong 0.6\,\mu$sec; $T_2^* \cong 0.8\,\mu$sec. τ_γ and $dH_0/dt = \gamma^{-1}\alpha$ were adjustable, respectively, over the ranges 0.1-0.8 μsec and 0.8-40 kilogauss/sec, giving a β range 0.001-0.06. Equation (2) should apply best to Fig. 3. The linearization $M_z \cong -M_0$ of Eq. (1) holds reasonably for Fig. 3 but marginally for Fig. 2. In spite of small β, and nonlinearity, even Fig. 1 has some features in common with Eq. (2). Modulation appears most marked just when Eq. (2) applies. The predicted period $T_n = (\pi/n\alpha)^{1/2}$ from (2), of the nth modulation period to appear, is correct within 50% for T_5 in Figs. 2 and 3. For the expected emission duration T, a useful rough estimate[2] is $2(\tau\tau_\gamma)^{1/2}\beta$, yielding reasonable values 500, 20, and 50 μsec for Figs. 1, 2, and 3, respectively.

We have shown that the maser oscillator emission envelope had in our case a structure dependent almost entirely on the field sweep. Though a simple pendulum-like energy exchange between cavity and emitting sample, described by the "general analysis" of SW, is a basic process,[2] it had nothing to do with our case, with either fast or slow H_0 sweep.

---

[1] J. R. Singer and S. Wang, Phys. Rev. Letters 6, 351 (1961).

[2] J. C. Kemp, thesis, University of California, Berkeley, 1960 (unpublished). The relevant portion is available as a University of California Report AFOSR-TN-60-509, issue 275, E.R.L., Berkeley, 1960 (unpublished).

[3] J. C. Kemp, J. Appl. Phys. 30, 1451 (1959). Though this paper covered the rather fundamental "pendulum nutation" mechanism (discussed earlier, without the nonlinearity, in reference 4), the possible role of H_0 sweep in actual experiments was not then appreciated. Adding line broadening to the static-parameter (static H_0) emission problem was discussed in this reference, in reference 5, and further in reference 2 (thesis only), and gives a possible lengthening of emission duration and a modulation frequency which can be smaller on the aver-

age but cannot increase with t over the envelope.

[4]N. Bloembergen and R. V. Pound, Phys. Rev. 95, 8 (1954). $\tau_\gamma^{-1} = \gamma M_0 Q/\mu_0 V$ (mks units[2]), where γ = magnetogyric ratio, M_0/V = available magnetization per unit cavity volume. In SW notation, $\tau_\gamma^{-1} = 4\pi N_e \gamma p Q$ or $4\pi N_e \gamma \mu Q$.

[5]See A. Yariv, J. Appl. Phys. 31, 740 (1960), who omitted a minor approximation (reference 2 Report, Appendix) leading to the pendulum equation, but gave a computer solution justifying our statement that the solution is quite like an exponentially decaying sinusoid.

[6]An unpublished waveform of P. F. Chester, P. E. Wagner, and J. G. Castle, Jr., Scientific Paper 6-94439-8-P4, Westinghouse Research Laboratories, Pittsburgh, Pennsylvania, 1958 (unpublished), p. 10, taken without H_0 sweep, shows the characteristic 100% almost uniform modulation, in my knowledge the only observed such case.

[7]It happened that $T_2^*/\tau \cong 1$ in our experiments. The mathematics can easily accommodate the more general case.

[8]E. T. Whittaker and G. N. Watson, Modern Analysis (Cambridge University Press, New York, 1935), 4th ed., pp. 347-351.

[9]Sweep-rate dependence of modulation depth was also noted by S. Foner, L. R. Momo, and A. Mayer, Phys. Rev. Letters 3, 36 (1959).

HELICITY OF μ^- MESONS; MOTT SCATTERING OF POLARIZED MUONS*

Marcel Bardon, Paolo Franzini,† and Juliet Lee
Columbia University, New York, New York
(Received June 13, 1961)

Current speculations[1] on weak interactions raise the possibility that the neutrino associated with the μ meson may be different from the neutrino of beta decay. Thus the helicity of ν_e may be different from that of ν_μ. This experiment was designed to observe the helicity of the μ^- meson (and hence that of the associated $\bar{\nu}_\mu$) from the reaction:

$$\pi^- \rightarrow \mu^- + \bar{\nu}_\mu . \qquad (1)$$

The method used was to analyze the polarization of the muons by Coulomb scattering of a transversely polarized μ^- beam (Mott scattering) which predicts a left-right asymmetry due to spin-orbit coupling:

$$\sigma(\theta, \phi) = f(\theta)[1 + g(\theta) P_y \cos\phi]. \qquad (2)$$

Here P_y is the transverse muon polarization, along the y axis, and the z axis is in the direction of the incoming muon momentum. Explicit calculations of the energy-dependent terms, $f(\theta)$ and $g(\theta)$, were performed by Rawitscher,[2] and by Franklin and Margolis.[3] Integration of the equation for the experimental arrangement used leads to a predicted asymmetry,

$$(L - R)/(L + R) = \pm 0.09 \text{ for } P_y = \mp 1, \qquad (3)$$

where L and R represent the number of scattering events into the left and right counters with respect to the plane defined by the μ momentum and spin.

Our results, corrected for accidentals and based on ~100 hours of counting ($\sim 3 \times 10^8$ muons), were $L = 515$ and $R = 618$. This leads to an asymmetry of -0.090 ± 0.031 for our $P_y = 0.9$, from which it is concluded that the helicity of the μ^- meson in reaction (1) is positive (right-handed) in agreement with the V-A theory. Thus the antineutrino in (1) is also right-handed, and hence no evidence is deduced from this result for $\nu_e \neq \nu_\mu$. This conclusion is in agreement with those obtained by measuring the knock-on electrons produced by high-energy longitudinally polarized μ mesons in magnetized iron.[4,5]

The agreement of predicted and observed asymmetry is interesting in that, to our knowledge, there are no pre-existing data on polarized electron or muon scattering in this momentum transfer region ($\langle \Delta q \rangle_{av} \sim 100$ Mev/c). More explicit discussion of this and of $\sigma(\theta)$ will be published later. We only note here that the inelastic scattering contribution is strongly limited by the low energy of the outgoing muon.

The Mott scattering experiment involved the extraction of a low-energy π^- beam, and the production from this beam of transversely polarized μ mesons by decay in flight. A magnetic channel was designed to this end, and its front inserted into a recessed window in the cyclotron vacuum chamber. The resulting beam of 43-Mev π mesons was further moderated by 3 in. of lithium, placed at the focus of a collimating magnetic system so as to produce a parallel ($\pm 2°$) beam of (28 ± 2.5)-Mev π mesons in the decay region. The resulting muons selected by decay angle had an average transverse polarization of 90% ($P_y = 0.9$) in the plane of decay, and were uniformly dis-

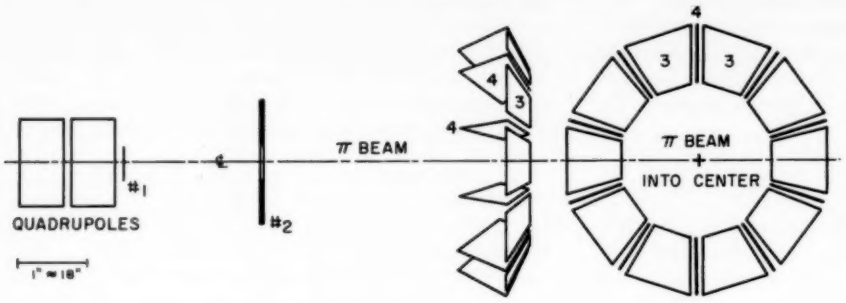

FIG. 1. Experimental setup showing disposition of beam counter No. 1, collimating counter No. 2, and wheel arrangement of ten sets of counters and lead scatterers.

tributed in energy from 9 to 33 Mev. This energy band was chosen as a compromise between intensity of backward scatterings and magnitude of asymmetry. The experimental arrangement (Fig. 1) makes use of the azimuthal symmetry of the pion decays in order to maximize the counting rate and minimize instrumental asymmetries. Lead was used as the scatterer and the scattering angles accepted were from 105° to 165°. The thickness of the lead was chosen for the greatest yield of events consistent with a not too substantial reduction of the asymmetry by plural scatterings.

The incoming muon is counted by a thin plastic counter (No. 3) and strikes a 2-g/cm² thick lead sheet. An event occurs when the muon is scattered back through No. 3 into either the left or the right No. 4 counters which are placed radially on either side of No. 3. This setup of counters and lead is repeated 10 times so as to form an annular arrangement about the pion beam as axis. The small scattering probability ($\sim 0.6 \times 10^{-5}$ per muon), together with a background of μ-mesonic x rays due to muons stopping in the lead, makes it necessary to further identify events by detecting the decay electrons from the scattered muons which are required to stop in the No. 4 counters ($\frac{3}{4}$ in. thick). Direct passage by a particle from the beam through No. 4 and then No. 3 is prevented by $\frac{3}{4}$-in. copper shields mounted on the edges of the No. 4 counters toward the beam.

Figure 2 shows a simplified block diagram of the fully transistorized electronics. The No. 2 counter was put in anticoincidence with No. 1, and ten such $1\bar{2}$ signals were obtained from an emitter follower fan-out system. Each was then put in coincidence with a signal from one of the ten No. 3 counters; the $1\bar{2}3$ then representing a μ^- meson which reached a particular set in the wheel. Each of these signals was sent to two emitter followers, and, as shown in Fig. 2, was counted in coincidence with a pulse from an adjacent No. 4 counter through a double-pole, double-throw relay. This device permitted the switching back and forth at regular intervals of the whole electronic chain following the $1\bar{2}3$ coincidence, thus eliminating some possible instrumental asymmetries. The $1\bar{2}34$ coincidence output was used to open a 3-μsec gate during which a pulse in No. 4, due to an electron from the decay of a stopped μ meson, would count as an event. Single counts in No. 4 gave accidental events which were about one-tenth of the true events. This low accidental rate was made possible by the use of the Nevis vibrating target,[6] which gave an average duty cycle of 3.

Instrumental asymmetries were rendered neg-

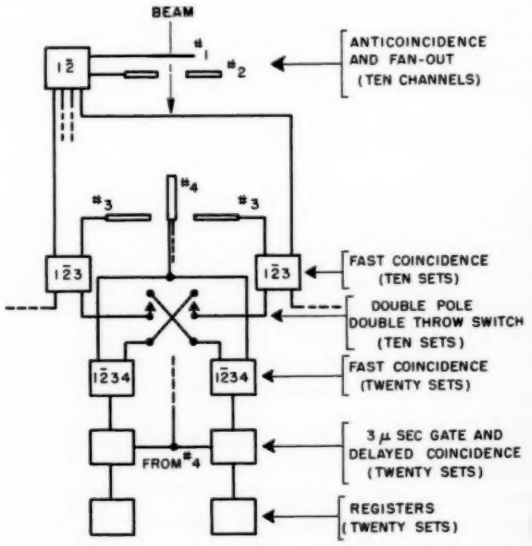

ligible by the following steps:

(i) During the 95 hours of counting, the electronic channels for left and right scattering were switched every hour.

(ii) The arrangement is such that each of the No. 4 counters is a "left" counter for one set and a "right" counter for the adjacent set.

(iii) The counters were aligned on the wheel to within ±0.016 in. around the 3-ft diameter. The repetitive pattern also serves to average out any residual asymmetry.

(iv) The wheel assembly was rotated about the π beam by one-fifth turn (incoherently) every two hours to smooth the small deviations from axial symmetry (beam shape and aim).

(v) Finally, a π^+ beam was scattered into the counters by 6 g/cm^2 of lead placed at No. 2 collimator. The π^+ mesons simulated true events by scattering back from the lead, stopping in No. 4 and giving a delayed electron via the $\pi^+ \to \mu^+ \to e^+$ chain. This yielded an inherent asymmetry (for almost isotropic scattering from Pb) of $+0.008 \pm 0.019$.

The authors wish to express their gratitude to Professor Leon M. Lederman for his continuous guidance and encouragement; and also to thank Uriel Nauenberg, Michael Tannenbaum, and the staff of the Nevis Cyclotron Laboratory for their assistance at various stages of the preparation of the experiment.

---

*This research was supported by the Office of Naval Research and the U. S. Atomic Energy Commission.

†Fulbright Fellow. On leave from University of Pisa, Pisa, Italy.

[1]See, for example, B. Pontecorvo, J. Exptl. Theoret. Phys. (U.S.S.R.) 37, 1751 (1959) [translation: Soviet Phys.—JETP 37(10), 1236 (1960)]; and also T. D. Lee and C. N. Yang, Phys. Rev. Letters 4, 307 (1960).

[2]G. H. Rawitscher, Phys. Rev. 112, 1278 (1958). We are particularly grateful to Professor Rawitscher for his kind loan of a computer program which we used in the calculations of scattering probabilities.

[3]J. Franklin and B. Margolis, Phys. Rev. 109, 525 (1958).

[4]A. E. Alikhanov et al., J. Exptl. Theoret. Phys. (U.S.S.R.) 38, 1918 (1960) [translation: Soviet Phys.—JETP 11, 1380 (1960)].

[5]G. Backenstoss, B. D. Hyams, G. Knop, P. C. Maria, and U. Stierlin, Phys. Rev. Letters 6, 415 (1961).

[6]J. Rosen, Bull. Am. Phys. Soc. 6, 9 (1961).

RELATIVE INELASTICITY AND ANISOTROPY OF PROTON INTERACTIONS AT 9 AND 23.5 Gev

E. M. Friedländer, M. Marcu, and M. Spîrchez

Cosmic-Ray Laboratory, Institute of Atomic Physics, Bucharest, Rumania

(Received June 15, 1961)

Recent observations of cosmic-ray jets[1] have brought evidence for a decrease of the inelasticity K of nucleon-nucleon collisions with increasing energy of the primary, together with an increase of the forward-backward peaking of the c.m. angular distribution of the secondaries.

In view of the obvious uncertainties connected with the estimation of primary energy and/or energy and identity of the created particles, we thought it desirable to check these trends under as far as possible controlled conditions at the highest available accelerator energies. We have measured K by two independent methods and found it to decrease significantly in the energy interval 9-25 Gev.

Electron pairs from π^0-2γ decay were detected by upstream scanning[2] along relativistic tracks: (1) in a stack of NIKFI-R pellicles, used in an earlier investigation,[3] irradiated in the internal beam of the Dubna proton-synchrotron circulating at 9-Gev total energy, and (2) in two Ilford G-5 pellicles irradiated in the external (scattered) momentum-analyzed beam of the CERN proton synchrotron (average momentum ~23.5 Gev/c). Only tracks with a projected length per plate ≥ 2 mm and a projected angle $\leq 30°$ with the beam direction were accepted. For each detected pair the projected opening angle α and the angle θ of the pair bisector with the beam direction were recorded. Since at least one electron track in each pair was essentially flat, the quantity $\langle \alpha^{-1} \rangle$ is proportional to the average π^0 energy within the accepted solid angle interval. In order to obviate the well-known difficulties connected with the estimation of the proportionality factor,[4] we preferred to compare directly $\langle \alpha^{-1} \rangle$ from the

two stacks, since

$$\frac{K_{23.5}}{K_9} \leq \frac{9}{23.5} \frac{\langle \alpha^{-1} \rangle_{23.5}}{\langle \alpha^{-1} \rangle_9} \frac{\langle n_\pi \rangle_{23.5}}{\langle n_\pi \rangle_9}, \quad (1)$$

the inequality sign in (1) being due to the stronger collimation of the secondaries at the higher energy. Using the experimental results on $\langle \alpha^{-1} \rangle$ given in Table I and the charged-pion multiplicities detected in along-the-track scans,[5,6] we obtain

$$K_{23.5}/K_9 \leq 0.70 \pm 0.08. \quad (2)$$

The quantities $\langle \alpha^{-1} \sin\theta \rangle$, which are a measure of the average transverse momentum of the neutral pions, are also given in Table I. The absence of any significant difference in the transverse momenta, as well as the practical independence of the transverse momentum on emission angle, allows an independent check of the above result by means of the charged secondaries.

Meson showers of at least three relativistic prongs and $N_h \leq 4$ were collected by an area scan, and the angular distribution of the shower tracks was measured. The condition $N_h \leq 4$ selected light target nuclei[3] and provided us with a sample enriched in proton-nucleon collisions. No effort was made to detect $N_h = 0$ stars in this run.

Provided p_T is independent of emission angle, we have

$$\frac{K_{23.5}}{K_9} = \frac{9}{23.5} \frac{\langle \csc\theta_s \rangle_{23.5}}{\langle \csc\theta_s \rangle_9} \frac{\langle n_\pi' \rangle_{23.5}}{\langle n_\pi' \rangle_9}, \quad (3)$$

where θ_s are the emission angles of the relativistic secondaries with respect to the incoming proton, and $\langle n_\pi' \rangle$ is the average multiplicity of shower tracks in the analyzed showers ($n_s \geq 3$).

Table I. Comparative data from measurements at 9 and 23.5 Gev.

Stack	9 Gev	23.5 Gev
No. of electron pairs	504	102
$\langle \alpha^{-1} \rangle$	251 ±11	273 ±27
$\langle \alpha^{-1} \sin\theta \rangle$	37 ±4	35 ±4
No. of stars with $n_s \geq 3$, $N_h \leq 4$	616	67
No. of tracks	2281	441
$\langle n_\pi' \rangle$	4.33 ±0.05	4.92 ±0.23

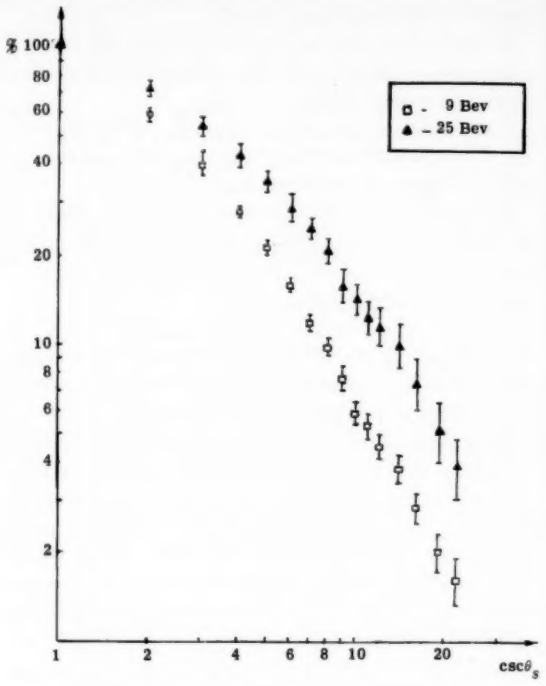

FIG. 1. Integral normalized distributions of $\csc\theta_s$ for 9-Gev meson showers (squared points) and 23.5-Gev meson showers (circles) with $n_s \geq 3$, $N_h \leq 4$.

The (normalized) integral distributions of $\csc\theta_s$ are shown in Fig. 1. The pertinent numerical data are also given in Table I and yield

$$K_{23.5}/K_9 = 0.67 \pm 0.06, \quad (4)$$

a result quite consistent with that from the π^0 measurement. Using the upper limit for the inelasticity at 9 Gev, deduced in reference 4, we obtain

$$K_{23.5} \leq 0.23 \pm 0.06. \quad (5)$$

In order to check the peaking of the c.m. angular distribution, an anisotropy parameter,

$$\eta \equiv (\tfrac{1}{2}\pi)^{1/2} (\sum |\ln \cot\theta_s - \langle \ln \cot\theta_s \rangle|) [n_s(n_s - 1)]^{-1/2}, \quad (6)$$

was computed for every shower with no relativistic prong in the backward hemisphere. It can be shown that if the quantities $\ln \cot\theta_s$ belong to a normal population of variance σ^2, then

$$\langle \eta \rangle = \sigma, \quad (7)$$

and

$$\sigma_\eta = 0.75\,\eta\, n_s^{-1/2}. \qquad (8)$$

The distributions of the η values for 9-Gev and 23.5-Gev showers are shown in Fig. 2 normalized to the same area. The marked shift towards higher η values at the higher energy is proved to be significant by a Pearson test ($\chi^2 = 20.5$ with 6 degrees of freedom). The average values are

$$\langle\eta\rangle_{23.5} = 0.54 \pm 0.02,$$

$$\langle\eta\rangle_{9} = 0.42 \pm 0.01, \qquad (9)$$

and prove that both distributions are significantly peaked (0.39 would be expected for isotropy).

The above results, which are consistent with recent indirect evidence from counter experiments,[7,8] are suggestive of an increasing part played by peripheral collisions, involving "almost real" pions in the meson clouds of the collision partners.[9-12] The implications of these results will be discussed quantitatively in a forthcoming paper, based upon the model discussed in references 10 and 11.

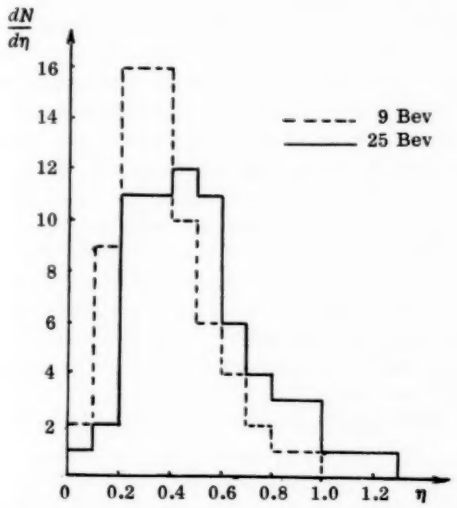

FIG. 2. Differential distributions of the anisotropy parameter η in the same showers. Dashed line at 9 Gev, full line at 23.5 Gev. The two histograms are normalized to the same area.

We are greatly indebted to Professor V. F. Weisskopf and Dr. W. O. Lock for making available the plates exposed at the CERN proton synchrotron, to Professor J. Ausländer for his support in this matter and for useful discussions, to H. Toţea for his assistance in processing the angular data, and to our scanner team for their wholehearted cooperation.

[1]See, e.g., D. H. Perkins, Progress in Cosmic-Ray Physics, edited by J. G. Wilson (Interscience Publishers, New York, 1960), Vol. 5; also L. Montanet, J. A. Newth, G. Petrucci, R. A. Salmeron, and A. Zichichi, Nuovo cimento 17, 166 (1960); S. Lal, Y. Pal, and A. Raghavan (to be published).

[2]D. I. King, Phys. Rev. 109, 1344 (1958).

[3]E. M. Friedländer, Nuovo cimento 14, 796 (1959).

[4]G. L. Bayatyan, I. M. Gramenitzkiĭ, A. A. Nomofilov, M. S. Podgoretzkiĭ, and E. Skrzypczak, Zhur. Eksp. i Teoret. Fiz. 36, 690 (1959) [translation: Soviet Phys.-JETP 36(9), 483 (1959)].

[5]I. M. Gramenitzkiĭ, M. Ia. Danysh, V. B. Liubimov, M. I. Podgoretzkiĭ, and D. Tuvdendorzh, Zhur. Eksp. i Teoret. Fiz. 35, 552 (1958) [translation: Soviet Phys.-JETP 35(8), 381 (1959)].

[6]G. Cvijanovich, B. Dayton, P. Egli, B. Klaiber, W. Koch, M. Nikolic, R. Schneeberger, H. Winzeler, J. C. Combe, W. M. Gibson, W. D. Lock, M. Schneeberger, and G. Vanderhaeghe (to be published).

[7]G. Cocconi, A. N. Diddens, E. Lillethun, and A. M. Wetherell, Phys. Rev. Letters 6, 231 (1961).

[8]M. Fidecaro, G. Gatti, G. Giacomelli, W. A. Love, W. C. Middelkoop, and T. Yamagata, Nuovo cimento 11, 382 (1961).

[9]N. Yajima, S. Takagi, and K. Kobayakawa, Progr. Theoret. Phys. (Kyoto) 24, 59 (1960).

[10]E. M. Friedländer, Phys. Rev. Letters 5, 212 (1960).

[11]F. Salzmann and G. Salzmann, Phys. Rev. Letters 5, 377 (1961).

[12]S. Dremin and D. Cernavsky (to be published).

SCATTERING OF 915-Mev α PARTICLES FROM CARBON AND HELIUM: DIRECT EVIDENCE FOR α-PARTICLE CLUSTERING IN NUCLEI*

Terence J. Gooding and George Igo
Lawrence Radiation Laboratory, University of California, Berkeley, California
(Received June 2, 1961)

We have obtained direct evidence for α-particle clustering in C^{12} from the $(\alpha, 2\alpha)$ reaction at 915 Mev. Measurements of the energies of the two outgoing α particles and the angular correlation between them show that the reaction proceeds via a direct collision between the incident α particle and an α-particle cluster in the nucleus. An estimate of the preformation probability has been obtained by comparing the carbon and helium differential cross sections.

Figure 1(a) is a diagram of the experimental arrangement. The 915-Mev α-particle beam from the Berkeley synchrocyclotron was focused at the center of an 18-in. diam scattering chamber to a spot 1 in. wide by 3/4 in. high. The beam intensity was about 3×10^8 α particles per sec and was monitored by an 8-in. diam ionization chamber. The duty cycle was increased from about 60 μsec per burst to 12 msec per burst by means of an extra peripheral dee. Measurements were made first with the chamber filled to 65 psi of helium and then with a thin graphite target (~260 mg/cm^2 for $\theta_L = 17$ deg and ~600 mg/cm^2 for $\theta_L = 26$ deg) placed at the center of the scattering chamber.

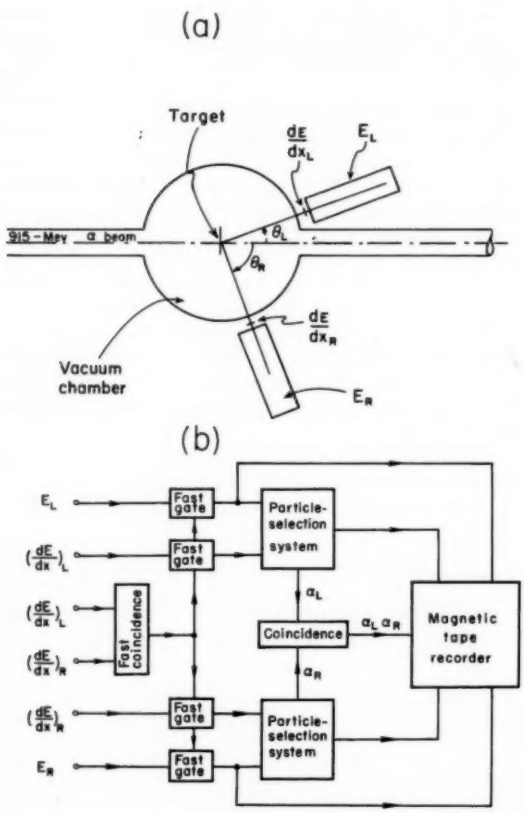

FIG. 1. (a) Diagram of the experimental arrangement. (b) Block diagram of the electronics.

Particles scattered from the target were detected by counters placed at angles θ_L and θ_R with respect to the α-particle beam. The particles were identified by measuring their total energy, E, and their rate of energy loss, dE/dX. The dE/dX counters were disks of plastic scintillator, 1.0 in. diameter by 0.1 in. thick, and the E counters were cylinders of plastic scintillator, 3.5 in. diameter by 11 in. long. The response of the counters to α particles and protons of various energies was determined by placing the counters, preceded by an appropriate absorber, in the direct α-particle and proton beams. The response was in reasonable agreement with calculations based on the response of plastic scintillator to lower energy protons, deuterons, and electrons.[1] The nuclear absorption in the E counters was about 35% and was determined in the direct beam by measuring the low-energy tail of the pulse-height spectrum.

A block diagram of the electronics is shown in Fig. 1(b). The fast-coincidence resolving time was 5 nsec and was limited by the flight-time difference between high- and low-energy α particles leaving the target. The particle-selection systems consisted of complex arrangements of discriminators and coincidence circuits acting on linear outputs from the dE/dX and E counters. In this way, we were able to sort doubly charged particles (He^3 and He^4) from singly charged particles with a high degree of reliability. Outputs from the particle selection systems were fed into a slow-coincidence unit which was used to start a magnetic recorder. With the helium target, the fast-coincidence counting rate was typically one per second, whereas the $(\alpha, 2\alpha)$ coincidence rate was only one per minute. Outputs from the E counters were pulse-height analyzed in the magnetic re-

corder. In addition, information concerning the energy range in which each α particle fell was recorded. The magnetic tape was subsequently analyzed using an IBM-7090 computer.

The differential cross section $d^2\sigma/d\Omega_1 d\Omega_2$ for scattering of the α-particle beam by helium and carbon was measured at $\theta_L = 17$, 26, and 45 deg, with $\theta_L + \theta_R = 87$ deg (the separation angle for elastic scattering at 915 Mev). At each angle, we measured the energy spectrum E_L and the spectrum of the sum of the energies $E_L + E_R$.

The spectra from helium at 17 deg are shown in Fig. 2. The peak at 815 Mev in E_L and 915 Mev in $(E_L + E_R)$ corresponds to the elastically scattered group. The second peak at $E_L = 650$ Mev and $(E_L + E_R) = 750$ Mev is thought to be due to stripping of the forward-going α particle into a He^3 plus a neutron. The relative intensities of these two peaks are misleading, since the elastic peak is sharply correlated at these angles, whereas the inelastic group would be expected to have a broader distribution. The third peak may be due to an energy cutoff in the experiment at around 350 Mev. The energy calibration throughout these measurements is uncertain to ±50 Mev. At 26 deg the spectrum looked essentially the same but the cross section was reduced. The cross section at 45 deg was too low to be measured.

The carbon data at 26 deg are shown in Fig. 3. The summed spectrum again shows two peaks, but the relative intensity of the elastically scattered group appears reduced. This is because the angular correlation is broadened by the momentum distribution of the α particles in the carbon nucleus. The peak at 750 Mev in the energy spectrum E_L for events with $E_L + E_R > 850$ (i.e., the elastically scattered group) shows clearly that the reaction is proceeding via a direct collision of the α particle with an α cluster in the nucleus. If, for instance, the initial collision was between the incident α particle and a deuteron, then the energy of the α particle scattered at 26 deg would be about 500 Mev. An α-particle–nucleon collision producing an α particle at 26 deg is kinematically forbidden.

Further evidence in support of this conclusion is given in Fig. 4 which shows the summed spectra for $\theta_L = 17$ deg and $\theta_L + \theta_R$ equal to (a) 87 deg and (b) 57 deg. The intensity of the quasi-elastically scattered group drops by about a factor of four when the separation angle is moved 30 deg from the kinematic angle of 87 deg. Consequently,

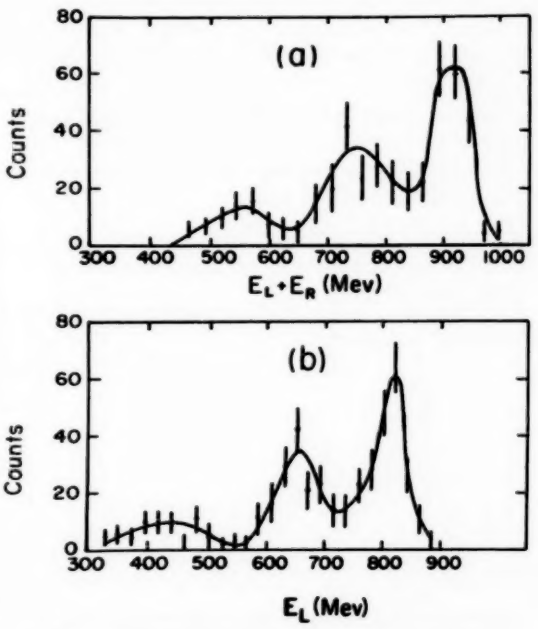

FIG. 2. Scattering from helium at $\theta_L = 17$ deg, $\theta_L + \theta_R = 87$ deg. (a) Summed energy spectrum $E_L + E_R$; (b) energy spectrum E_L. The energy calibration is uncertain to ±50 Mev.

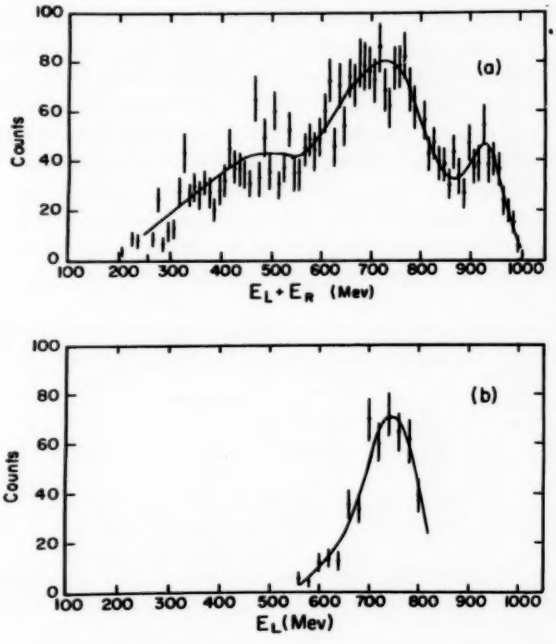

FIG. 3. Scattering from carbon at $\theta_L = 26$ deg, $\theta_L + \theta_R = 87$ deg. (a) Summed energy spectrum $E_L + E_R$; (b) energy spectrum E_L, where $E_L + E_R > 850$ Mev. The energy calibration is uncertain to ±50 Mev.

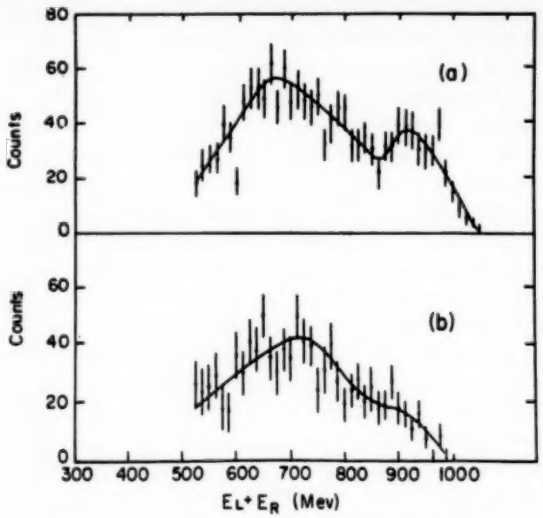

FIG. 4. The carbon summed energy spectrum at $\theta_L = 17$ deg and (a) $\theta_L + \theta_R = 87$ deg; (b) $\theta_L + \theta_R = 57$ deg. The energy calibration is uncertain to ±50 Mev.

the recoil α particle is correlated to within $(6 \pm 3)\%$ of the total available solid angle.

In order to obtain the probability of α-particle clustering in carbon, the differential cross sections for elastic scattering from helium and quasi-elastic scattering from carbon have been calculated at 17, 26, and 45 deg and are shown in Table I. The differential cross section for helium has been corrected for the finite size of the beam, the finite extent of the helium gas target, and nuclear absorption in the counters. To obtain the cross section for carbon, one must integrate over the solid angle into which the correlated α particle can be scattered.

To perform this integration, we have assumed that the angular correlation follows a triangular

Table I. The differential cross sections for elastic scattering from helium and quasi-elastic scattering from carbon.

θ_L (deg)	$d\sigma/d\Omega$ (μb/sr) Helium	$d\sigma/d\Omega$ (μb/sr) Carbon	$\frac{d\sigma/d\Omega \text{ (carbon)}}{d\sigma/d\Omega \text{ (helium)}}$
17	165 ±35	287 ±150	1.7 ±0.9
26	22 ±11	86 ±50	3.9 ±2.9
45	~0	~0	...

distribution through the two experimental points, that the angular correlation at $\theta_L = 26$ deg is the same as at $\theta_L = 17$ deg, and that the width of the distribution out of the plane of scattering is the same as that in the plane of scattering. The large errors on the cross sections quoted in Table I are primarily due to the inadequacy of the data on the angular-correlation function.

The ratio of the $(\alpha, 2\alpha)$ differential cross section for carbon and helium is 1.74 ± 0.9 at 17 deg and 3.9 ± 2.9 at 26 deg. According to the extreme α-particle model for carbon, we would expect this ratio to be about 3.

Further measurements are in progress on the angular-correlation function and the differential cross section for the $(\alpha, 2\alpha)$ reaction for other nuclei.

We wish to thank Charles A. Corum for designing the scattering chamber, Melvin Brown and Ellwood S. Douglas for assistance with the electronics, Dr. Paul Concus for the computer program, and the crew of the 184-in. cyclotron for their cooperation.

*This work was supported by the U. S. Atomic Energy Commission.

[1]T. J. Gooding and H. G. Pugh, Nuclear Instr. and Methods 7, 189 (1960).

NUCLEAR DE-EXCITATION FOLLOWING MUON CAPTURE AND THE BOUND MUON DECAY ANOMALY*

Frank Chilton
University of Washington, Seattle, Washington
(Received June 9, 1961)

Experiments have been performed[1-3] to measure the rate of negative muon decay,

$$\mu^- \rightarrow e^- + \nu + \bar{\nu},$$

when the muon is bound in the Coulomb field of a nucleus. Figure 1 presents the data of Yovanovitch[1] for the ratio of the bound decay rate to the free decay rate (rate for μ^+ decay or rate for muons bound to a low-Z nucleus),

$$R = \Lambda_d^-/\Lambda_d^+.$$

The curve is a theoretical curve.[4] While the theoretical predictions are always less than $R = 1$ the experimental results rise well above $R = 1$ in the iron region, yet return quickly close to theory for $_{30}$Zn, and fall well below the theoretical curve for very large Z. The presence of this anomaly has been verified in detail by combining measurements by Lederman and Weinrich[2] of Λ_d^-/Λ_t and measurements of Λ_t,[3] the total disappearance rate. These points are not included in Fig. 1 simply to avoid clutter.

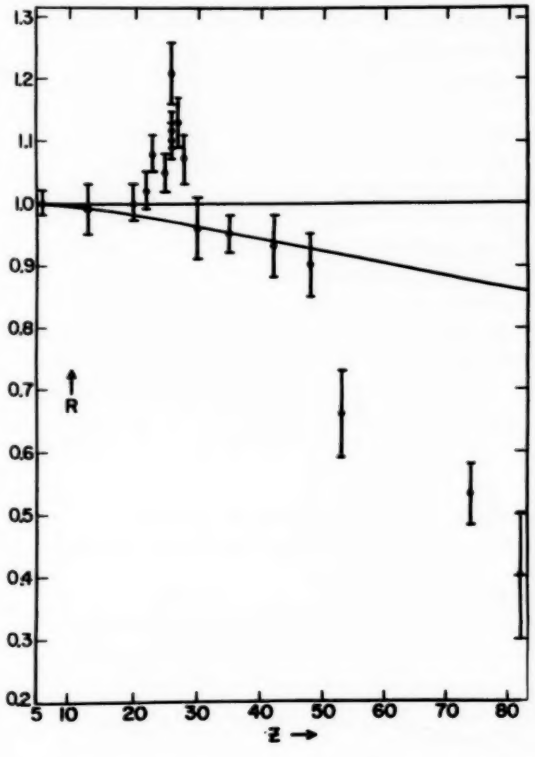

FIG. 1. Data of Yovanovitch (reference 1) on bound muon decay.

The other mode of disappearance of negative muons in matter is muon capture for which the basic reaction is

$$\mu^- + p \rightarrow n + \nu.$$

To determine whether the bound muon decay anomaly is really due to detection of γ rays associated with muon capture rather than electrons from muon decay, we can take the difference between the experimental and theoretical values for R and divide by Λ_c/Λ_d^+. Table I presents the values of $(R_{\text{exp}} - R_{\text{th}})\Lambda_d^+/\Lambda_c$ calculated using experimentally determined capture rates.[5] The near constancy of the values in Table I makes it appear that the anomaly is due to the detection of 1% of the muon capture events and that this sensitivity to muon capture mysteriously stops at Zn. The initially sharp Z dependence of the anomaly is just the Z dependence of muon capture rates $\sim Z^4$.

To understand how background due to muon capture could appear in such careful experiments, let us consider some of the nuclear processes

Table I. Proportionality of the bound muon decay anomaly to the capture rate.

Z	Element	$(R_{\text{exp}} - R_{\text{th}})\Lambda_d^+/\Lambda_c$ ($\times 10^2$)
20	Ca	0.4 ±0.5
22	Ti	0.7 ±0.5
23	V	1.5 ±0.4
25	Mn	1.0 ±0.4
26	Fe	1.4 ±0.3
26	Fe	1.7 ±2.0[a]
27	Co	1.3 ±0.3
28	Ni	0.8 ±0.3
29	Cu	1.2 ±0.9[a]
30	Zn	-0.1 ±0.2

[a]From measurements of Λ_d^-/Λ_t by Lederman and Weinrich (reference 2).

accompanying muon capture in complex nuclei. For capture by a free proton the recoil neutron has an energy of 5 Mev. In complex nuclei the average nuclear excitation is 10 to 15 Mev depending on the nuclear model.[6-8] All but about 2 Mev is imparted to the neutron.

When the neutron excitation is greater than the neutron separation energy, neutron emission is usually most likely. From the experimental cross sections for (n,γ) reactions, which are typically a few millibarns,[9] and from experimental cross sections for neutron scattering, which are typically a few barns, the ratio of the photon to neutron emission rates is

$$\Gamma_\gamma/\Gamma_n \sim 10^{-3},$$

when the excitation is a few Mev above the neutron separation energy. In particular this indicates that in this energy region the emission of photons with $E_\gamma > 10$ Mev is unlikely.[10,11] Other properties of neutron emission have been considered in connection with the problem of the neutron asymmetry from the capture of polarized muons.[7,12,13]

When the neutron excitation energy is less than the separation energy, only de-excitation by photon emission is possible. Note that this situation can occur as the second stage of compound nuclear decay even when the initial excitation is greater than the separation energy. Also note that compound nuclear processes are expected to prevail over direct neutron emission.[13] While it would certainly be difficult to calculate the photon spectrum that results from muon capture, a great deal of qualitative information can be obtained from experimental data on the γ-ray spectra resulting from thermal neutron capture.[14] This corresponds to an excitation close to the separation energy, the highest excitation resulting only in photon emission. We have already seen that this situation occurs with sufficient probability.

The first thing to be learned from thermal neutron capture is an estimate of the mean multiplicity of photons. This varies between 2.5 to 4 photons per capture for the medium-weight nuclei, depending on the nucleus involved. The mean multiplicity for muon capture might be expected to be slightly higher for each nucleus than its thermal neutron counterpart since the excitation takes place in such a different way and because the more favored states in muon capture differ from those of photon emission. The "allowed" and "first forbidden" transitions in muon capture correspond to 0+, 1+ and 0-, 1-, 2- transitions, respectively.[15] However, since $k_\nu R \sim 2.5$ for medium nuclei, a change of two units of forbiddenness should make a difference of no more than about 10^{-2} in the transition probability.[15] The most important consideration is which states are available.

Another thing to be learned from neutron capture is the presence of strong direct transitions in certain regions of the periodic table. In the iron region there are strong direct $s \rightarrow 2p_{3/2}$ transitions. An example, the thermal neutron capture spectrum of Fe^{57}, is shown in Fig. 2. The $E_\gamma = 7.65$ Mev, 40% frequency peak corresponds to a transition to the $2p_{3/2}$ single-particle state. The smaller $E_\gamma = 6.0$ Mev peaks correspond to the $2p_{1/2}$ state. For reasons discussed below, the bound muon decay anomaly seems to be due to γ rays with 5 Mev $\leq E_\gamma \leq$ 10 Mev. The experimental anomaly in muon decay found in the iron region suggests that these same p states seem to play an important role in the γ-ray transitions that cause the anomaly. This is illustrated by the

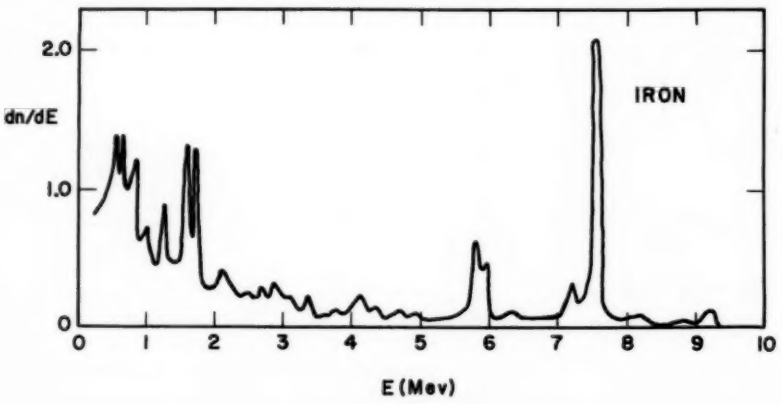

FIG. 2. Thermal neutron capture γ-ray spectrum of Fe (from reference 14).

cases

$$_{28}Ni^{58,60}(\mu^-,\nu)_{27}Co^{58,60*},$$

and

$$_{30}Zn^{64,66,68}(\mu^-,\nu)_{29}Cu^{64,66,68*},$$

for which the final nuclei have the $p_{3/2}$ states essentially full.[16] Table I indicates that the bound muon anomaly is diminished for $_{28}$Ni and gone for $_{30}$Zn, but not for $_{27}$Co or $_{29}$Cu for which the daughter nuclei have empty $p_{3/2}$ states. The single-particle states which would seem most favorable to production of such γ rays in muon capture are listed in Table II for a few nuclei. This is based on the fact that the outermost proton shells are the most important in muon capture,[12] and on considerations of the relative contributions of the various states involved.[17,18] Configuration mixing is apparently responsible for making the p states important, which is consistent with evidence[19] for the applicability of the Nilsson model[20] in the iron region. It is clear from Table II that the yield of higher energy γ rays resulting from muon capture in Ni and Zn will be less than that in the remainder of the iron region. It is also understandable why the anomaly disappears at $_{30}$Zn; the $2p_{3/2}$ proton shell is being filled but the $2p_{3/2}$ neutron shell is already full. However, note that the anomaly might still be expected to be present for $_{29}$Cu although in possibly reduced intensity because the shells are partially filled. The data of Lederman and Weinrich[2] are consistent with this (see Table I).

The experimental arrangement of Yovanovitch[1] included a thick target and an electron telescope consisting of three thin plastic scintillators with two aluminum absorbers sandwiched between the scintillators. The absorber thickness was equal to the range of a 4-Mev electron. The arrangement of Lederman and Weinrich was similar.[2] A 5- to 10-Mev γ ray can produce either a pair or a Compton electron with energy >4 Mev in either the target or the first absorber which will be detected by two counters. In coincidence, a Compton electron from a low-energy γ ray can be detected in the remaining counter. From the known cross sections[21] the total efficiency for such a high-low combination as that above is probably close to 1%, primarily because there are several different ways in which this event can take place. The discrepancy for large Z is evidently due to the different effect of thick targets and absorbers on the altered electron spectrum for bound muon decay as opposed to the spectrum for free decay.[22]

Whether or not the above mechanism is responsible for the bound muon decay anomaly can be tested experimentally. Use of an experimental method which absolutely guarantees exclusion of electrons and photons with $E<10$ Mev would demonstrate whether the anomaly must be due to other effects than muon decay. This seems to be the case.[23] Anderson et al.[11] have measured the γ-ray spectra from muon capture in Fe and Cu. The part of the spectrum with $E_\gamma>5$ Mev does not seem inconsistent with the above ideas. The contrast in the γ-ray spectra in the iron region with that in and after Zn should be particularly interesting. Whether the high-low combination of γ rays is likely following muon capture could be determined by a coincidence experiment. Performing an experiment similar to that of Yovanovitch[1] and Lederman and Weinrich[2] with an electron telescope consisting of many counters would be particularly enlightening if all events were stored in which, for instance, the first and last counters register. Such an experiment would permit measurement of bound decay rates and examination of the detailed effects of photons from muon capture simultaneously.

It might also be expected that strong direct γ-ray transitions following muon capture show up

Table II. Expected dominant single-particle transitions resulting in γ rays with $E_\gamma>5$ Mev.

Nuclei	Initial proton state	Excited neutron state	Configuration mixing	Final neutron state	Comment
$_{26}Fe^{56}(\mu^-,\nu)_{25}Mn^{56*}$	$1f_{7/2}$ $1f_{7/2}$	$1g_{9/2}$ $1g_{9/2}$	$2d_{3/2}$ ···	$2p_{3/2}$ $1f_{5/2}$	
$_{28}Ni^{58,60}(\mu^-,\nu)_{27}Co^{58,60*}$	$1f_{7/2}$	$1g_{9/2}$	···	$1f_{5/2}$	Co^{60}, $p_{3/2}$ full Co^{58}, $(p_{3/2})^3$
$_{30}Zn^{64,66,68}(\mu^-,\nu)_{29}Cu^{64,66,68*}$	$2p_{3/2}$	$2d_{3/2}$	···	$2p_{1/2}$	$p_{3/2}$ full

in other regions of the periodic table. This should be most likely in the light nuclei and near closed shells as is the case in thermal neutron capture.

The author would like to thank Professor E. M. Henley for many helpful discussions, and Professor H. L. Anderson, Professor J. W. Keuffel, and Dr. R. W. Huff for notification of their results prior to publication.

---

*Work supported in part by the U. S. Atomic Energy Commission.

[1]D. D. Yovanovitch, Phys. Rev. 117, 1580 (1960). The problem has been briefly reviewed by V. L. Telegdi, Proceedings of the 1960 Annual International Conference on High-Energy Physics at Rochester (Interscience Publishers, Inc., New York, 1960), p. 724.

[2]L. M. Lederman and M. Weinrich, CERN Symposium on High-Energy Accelerators and Pion Physics (CERN, Geneva, 1956), Vol. 2, p. 427.

[3]W. A. Barrett, F. E. Holstrom, and J. W. Keuffel, Phys. Rev. 113, 661 (1959); W. B. Gilboy, Phil. Mag. 4, 1055 (1959).

[4]Approximate calculations of the decay rates for bound muons were performed by H. Überall, Phys. Rev. 119, 365 (1960); V. Gilinsky and J. Mathews, Phys. Rev. 120, 1450 (1960). Recently an exact calculation has been completed by R. W. Huff, R. H. Dalitz, and K. Smith, Bull. Am. Phys. Soc. 6, 269 (1961).

[5]J. C. Sens, Phys. Rev. 113, 679 (1959).

[6]J. Tiomno and J. A. Wheeler, Revs. Modern Phys. 21, 153 (1949).

[7]H. Überall, Nuovo cimento 6, 533 (1957).

[8]H. Primakoff, Revs. Modern Phys. 31, 802 (1959). H. A. Tolhoek, Nuclear Phys. 10, 606 (1959).

[9]Neutron Cross Sections, compiled by D. J. Hughes and R. B. Schwartz, Brookhaven National Laboratory Report BNL-325 (Superintendent of Documents, U. S. Government Printing Office, Washington, D. C., 1958), 2nd ed.; A. M. Lane and J. E. Lynn, Nuclear Phys. 11, 646 (1959).

[10]The points with $E > 10$ Mev reported by J. W. Keuffel, Proceedings of the 1960 Annual International Conference on High-Energy Physics at Rochester (Interscience Publishers, Inc., New York, 1960), p. 544, were due to neutrons; J. W. Keuffel (private communication).

[11]H. L. Anderson et al. (to be published) have measured the γ-ray spectrum from muon capture in Fe and Cu with negative results for $E_\gamma > 10$ Mev.

[12]E. I. Dolinsky and L. D. Blokhintsev, Nuclear Phys. 10, 527 (1959); M. K. Akimova, L. D. Blokhintsev, and E. I. Dolinsky, Nuclear Phys. 23, 369 (1961).

[13]Elihu Lubkin, Ann. Phys. 11, 414 (1960).

[14]See E. Troubetzkoy and H. Goldstein, Oak Ridge National Laboratory Report ORNL-2904, 1960 (unpublished), and the references cited therein. G. A. Bartholomew, Nuclear Spectroscopy, edited by Fay Ajzenberg-Selove (Academic Press, Inc., New York, 1960), Part A, p. 304.

[15]M. Morita and A. Fujii, Phys. Rev. 118, 606 (1960); M. Morita and D. Greenberg, Phys. Rev. 119, 435 (1960).

[16]J. P. Schiffer, L. L. Lee, and B. Zeidman, Phys. Rev. 115, 427 (1959).

[17]D. H. Wilkinson, Ann. Rev. Nuclear Sci. 9, 1 (1959).

[18]H. A. Tolhoek and J. R. Luyten, Nuclear Phys. 3, 679 (1957).

[19]J. F. Vervier and G. A. Bartholomew, Proceedings of the International Conference on Nuclear Structure, Kingston, Canada, edited by D. A. Bromley and E. W. Vogt (University of Toronto Press, Toronto, 1960), p. 650.

[20]S. G. Nilsson, Kgl. Danske Videnskab. Selskab, Mat.-fys. Medd. 29, No. 16 (1955).

[21]R. D. Evans, Handbuch der Physik, edited by S. Flügge (Spinger-Verlag, Berlin, 1958), Vol. 34, p. 218; W. Heitler, The Quantum Theory of Radiation (Oxford University Press, New York, 1954), 3rd ed., Chap. 7.

[22]R. W. Huff (private communication).

[23]J. W. Keuffel (private communication) has measured the electron energy and time dependence of bound muon decay in Fe for electrons with $E > 10$ Mev. The results are consistent with the calculations of Huff.

ANOMALY IN MESON PRODUCTION IN $p+d$ COLLISIONS*

Norman E. Booth, Alexander Abashian, and Kenneth M. Crowe
Lawrence Radiation Laboratory, University of California, Berkeley, California
(Received June 12, 1961)

In an earlier Letter[1] we reported the results of some preliminary measurements of the momentum spectra of He^3 and H^3 nuclei produced in collisions of high-energy (624- to 743-Mev) protons with deuterium. In addition to the single-pion reactions

$$p+d \rightarrow \begin{cases} He^3+\pi^0 & (1a) \\ H^3+\pi^+, & (2a) \end{cases}$$

we looked for the reactions

$$p+d \rightarrow \begin{cases} He^3+\omega^0 & (1b) \\ He^3+\pi^++\pi^- & (1c) \\ He^3+\pi^0+\pi^0, & (1d) \end{cases}$$

and

$$p+d \rightarrow \begin{cases} H^3+\omega^+ & (2b) \\ H^3+\pi^++\pi^0, & (2c) \end{cases}$$

where ω may be a particle of mass between 1 and 2.8 pion masses. For reactions resulting in a He^3, the two pions (or particle) can be in isotopic spin states 0 or 1; if a H^3 results, only $I=1$ is allowed. We found an anomalous peak in the He^3 spectra which appeared to behave kinematically like a particle or resonance of mass approximately 310 Mev. At that time we were unable to give a definite isotopic spin assignment to the anomaly, and we considered a P-wave π-π resonance as a possible explanation.[2]

We have since repeated the experiment with a new arrangement which enabled us to measure both the He^3 and H^3 spectra with improved resolution and accuracy. With the new data we have been able to assign an isotopic spin $I=0$ to the anomaly, and subsequently to rule out the P-wave π-π resonance hypothesis. It is possible to explain the anomaly by means of a strong S-wave π-π attraction in the $I=0$ state, with a scattering length between 2 and 3 pion Compton wavelengths.

Figure 1 is a schematic drawing of the experi-

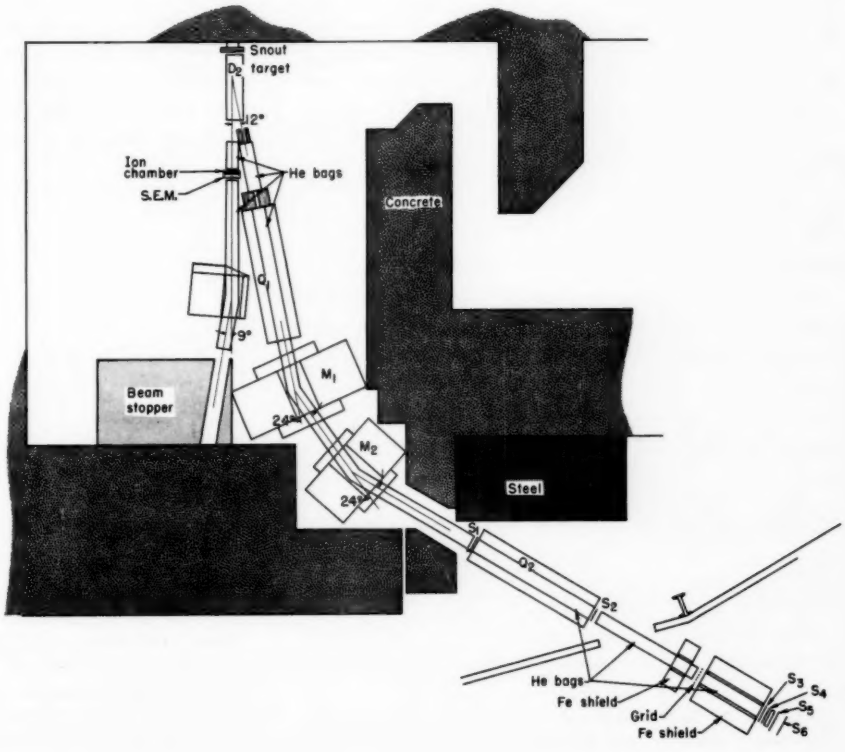

FIG. 1. Experimental arrangement.

mental arrangement. The proton beam extracted from the 184-inch cyclotron was passed through a gaseous deuterium target operated at liquid nitrogen temperature and at about 300 psi. Particles produced at 11.8 deg were collimated by a system of slits, and focused at infinity by the quadrupole Q_1. Momentum analysis was accomplished by the bending magnets M_1 and M_2. Quadrupole Q_2 focused the particles at a grid consisting of six $\frac{1}{2}$-inch-wide counters, each of which defined a momentum bite $\Delta p/p$ of 0.45%. He^3 and H^3 were selected from other particles by time of flight, range, and dE/dx. Backgrounds were measured by using hydrogen gas in the target.

The results of the measurements[3] of the He^3 and H^3 spectra at the full proton energy of 743 Mev are shown in Figs. 2(a) and 2(b). We were unable to observe He^3 of momenta less than 1000 Mev/c because of their low range. The peaks at 1530 Mev/c correspond to Reactions (1a) and (2a) at 50 deg c.m. for the heavy particle. The peak at 820 Mev/c in the H^3 spectrum corresponds to 156 deg c.m. in Reaction (2a). Double-pion production for this laboratory-system angle is kinematically possible between the limits of 910 and 1440 Mev/c.

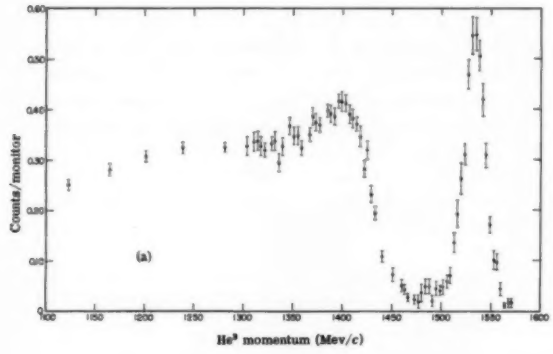

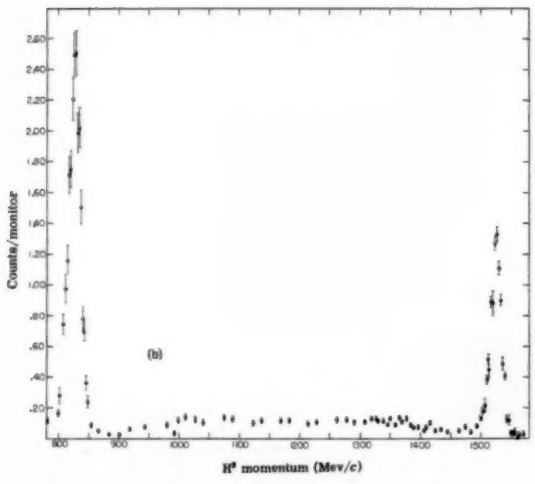

FIG. 2. (a) Momentum spectrum of He^3 at 11.8 deg, laboratory system. (b) Momentum spectrum of H^3.

If we assume the anomaly is not due to a pion-nucleon interaction, and that charge independence holds, we can analyze Reactions (1b), (1c), (1d), (2b), and (2c) in terms of the isotopic spin of the two pions (or particle). Since the $p+d$ system has $I=\frac{1}{2}$ and $I_z=\frac{1}{2}$, we can form with He^3 or H^3 the isotopic spin eigenfunctions having $I=\frac{1}{2}$, $I_z=\frac{1}{2}$:

$$\Pi_0{}^0 He^3, \tag{3a}$$

$$(\tfrac{2}{3})^{1/2}\Pi_1{}^1 H^3 - (\tfrac{1}{3})^{1/2}\Pi_1{}^0 He^3, \tag{3b}$$

where, for two pions,

$$\Pi_1{}^1 = (\tfrac{1}{2})^{1/2}(\pi^+\pi^0 - \pi^0\pi^+), \tag{4a}$$

$$\Pi_1{}^0 = (\tfrac{1}{2})^{1/2}(\pi^+\pi^- - \pi^-\pi^+), \tag{4b}$$

and

$$\Pi_0{}^0 = (\tfrac{1}{3})^{1/2}(\pi^+\pi^- + \pi^-\pi^+ - \pi^0\pi^0). \tag{4c}$$

Thus, with H^3 we have only $I=1$ production; but with He^3 we have both $I=0$ and $I=1$, the amount of $I=1$ being $\frac{1}{2}$ as large as in the H^3 case. To get the $I=0$ spectrum shown in Fig. 3, we drew a smooth curve through the H^3 spectrum, divided it by two, and subtracted it from the He^3 spectrum.

Before looking carefully into possible explana-

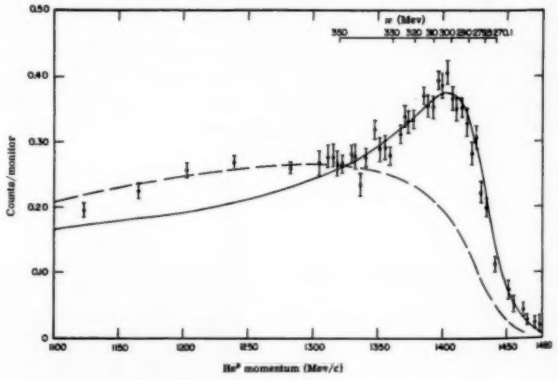

FIG. 3. $I=0$ part of He^3 spectrum. The dashed curve is the phase-space volume fitted to the points below 1300 Mev/c. The solid curve is the phase-space volume multiplied by the pion-pion enhancement factor for a scattering length $a_{S0}=2.8\hbar/\mu c$. The experimental resolution has been folded into both curves. The w scale gives the total energy in the two-pion barycentric system.

tions for the bump that appears in the $I=0$ spectrum, one must know the momentum resolution of the experiment. This resolution was calculated by taking into account such effects as finite angular definition, beam dimensions, image and grid sizes, multiple scattering, angular divergences, and energy spread of the proton beam. By making reasonable assumptions about the energy spread of the proton beam, we were able to reproduce the shapes and widths of the three single-pion production peaks. Figure 4 shows the resolution function for He^3 momenta near 1400 Mev/c. The full width at half maximum is 35 Mev/c, with an estimated uncertainty of $^{+6}_{-2}$ Mev/c.

As a starting point for comparing the data with theory, we computed the Lorentz-invariant phase-space volume element in the laboratory system:

$$\phi_s = \frac{d^2\rho}{dp_3 d\Omega_3} = \frac{p_3^2}{\omega_3}\left(1 - \frac{4\mu^2}{w^2}\right)^{1/2}, \tag{5}$$

where

$$\rho \propto \int \frac{d\vec{p}_3}{\omega_3}\frac{d\vec{p}_4}{\omega_4}\frac{d\vec{p}_5}{\omega_5}\,\delta(\vec{p}_3+\vec{p}_4+\vec{p}_5-\vec{p}_1)\,\delta(\omega_3+\omega_4+\omega_5-W_L),$$

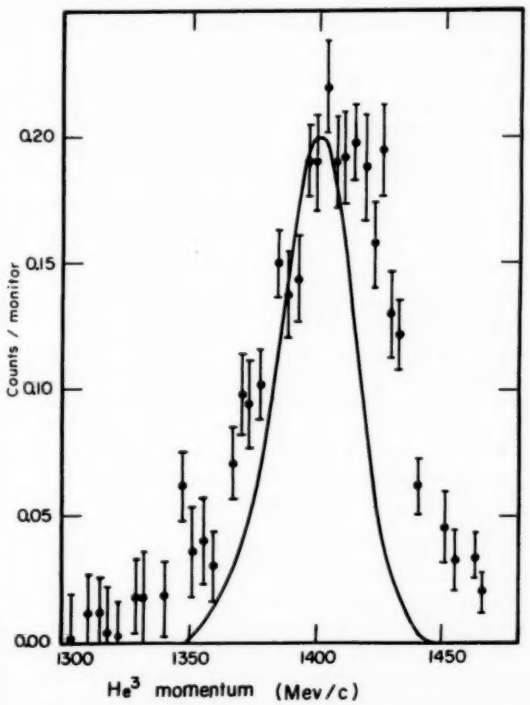

FIG. 4. Effect of subtracting the phase-space volume from the $I=0$, He^3 data. The solid curve is the computed experimental resolution at 1400 Mev/c.

$\vec{p}_1$ is the momentum of the incoming proton, W_L is the total energy in the laboratory system, p_3 and ω_3 are the respective momentum and total energy of the He^3, and w is the total energy in the barycentric system of particles 4 and 5, the two pions of mass μ. We have assumed the transition matrix element to be a constant, and restrict ourselves to the relativistically invariant form of the volume in phase space. The calculations were done for charged and neutral pions and combined according to Eq. (4c). With the resolution folded in and normalized to the experimental data at momenta below 1350 Mev/c, ϕ_S is shown as the dashed curve in Fig. 3.

A promising explanation at the moment is that the anomaly is due to a strong S-wave π-π interaction[4] that can be characterized by a scattering length. The conditions for the validity of the theory of final-state interactions[5] are: that the mechanism of the primary reaction be a short-range interaction, that the final-state interaction be strong and attractive, and that we consider only low relative energies of the two pions. Under these conditions, which we will see can be satisfied here, the volume element in phase space [Eq. (5)] for a given value of the pion-pion energy w is enhanced by a factor proportional to the pion-pion scattering cross section at the energy w. To obtain the energy dependence of the pion-pion cross section we go to Eq. (V.22) of Chew and Mandelstam,[6] where we define a scattering length a_{s0} as the amplitude at zero energy. We have

$$\left(\frac{\nu}{\nu+1}\right)^{1/2}\cot\delta_0^{\,0} = \frac{1}{a_{s0}} + \frac{2}{\pi}\left(\frac{\nu}{\nu+1}\right)^{1/2}\ln\left[\nu^{1/2}+(\nu+1)^{1/2}\right], \tag{6}$$

where $\delta_0^{\,0}$ is the S-wave π-π phase shift in the $I=0$ state and ν is the square of the momentum (in pion mass units) in the two-pion barycentric system. This gives an enhancement factor (normalized to unity at $\nu=0$),

$$F(\nu) = \left\{\left[1 + \frac{2a_{s0}}{\pi}\left(\frac{\nu}{\nu+1}\right)^{1/2}\ln\left[\nu^{1/2}+(\nu+1)^{1/2}\right]\right]^2 + a_{s0}^{\,2}\left(\frac{\nu}{\nu+1}\right)\right\}^{-1}. \tag{7}$$

This is exact for the S-dominant solutions of the π-π equations[7] where the π-π coupling constant is

$$\lambda = -\tfrac{1}{3}\frac{a_{s0}}{1+0.554\,a_{s0}}.$$

For the P-dominant solutions[8] Eq. (7) is still a very good approximation, but to evaluate λ we must know ν_R and Γ, the position and width parameters, respectively, of the P-wave π-π resonance.[9] We obtained good fits to our $I=0$ data at momenta above 1350 Mev/c with a_{S0} between 2.2 and 3.0$\hbar/\mu c$ with a best-fit value of 2.5$\hbar/\mu c$. The solid curve of Fig. 3 shows the fit obtained for $a_{S0}=2.8\hbar/\mu c$. We do not expect the computed curve to fit the experimental points below 1350 Mev/c for the following reason: The final-state interaction picture is valid only at low relative energies of the two pions where their attraction is large compared to other effects, such as details of the production mechanism and final-state π-He^3 interactions.

In Fig. 4 we show the result of subtracting the phase-space volume from the data. The peak occurs at a mass value of about 300 Mev, and unfolding the resolution gives a width of about 25 Mev. This yields a lifetime of the same order as the interaction time, and the concept of a particle becomes vague. It therefore seems doubtful that this is the vector meson of Nambu.[10] We intend to settle this question independently of the resolution in a subsequent experiment.

We cannot completely rule out the possibility that the anomaly is due to final-state interactions between the He^3 and one of the pions. The $I=\frac{3}{2}$, $J=\frac{3}{2}$, pion-nucleon state can occur in the H^3 case, but not as strongly as in the He^3 case. However, in the region of the anomaly we are below the energy of the $\frac{3}{2}$, $\frac{3}{2}$ resonance. Also, in other experiments in which the final state consists of two pions and a nucleon, the energy spectrum of the nucleon is usually not strongly influenced by the $\frac{3}{2}$, $\frac{3}{2}$ resonance.[11] We can dismiss the S-wave pion-nucleus interaction because it is known to be small at these energies.[12]

We have also considered the symmetrization of the wave function for the two pions. Details of the derivation are given in reference 3. We present here only the result, which is to multiply Eq. (5) by the factor $B(R)=1+\exp\{-[(w/\mu)^2-4]\times(R/2.15)^2\}$, where R is the radius of interaction in units of $1/\mu$. The effect of the symmetrization on the shape of ϕ_S is small for all values of R and cannot reproduce the observed bump. We will therefore neglect $B(R)$, although including it would decrease the value of the scattering length derived above.

Another effect we mention only briefly is the He^3 wave function. Roughly speaking, the three nucleons stick together to form a He^3 more easily when they have low relative energies because the He^3 wave function has fewer high-momentum components. This effect favors low He^3 momenta. From both the H^3 and He^3 spectra, we conclude that this effect is small or else compensated for by something else.

We plan to repeat the experiment at another laboratory-system angle. It should then be possible to make the correct interpretation.

We wish to acknowledge the generous and helpful assistance of the many students, notably Robert L. Beck, Philip B. Beilin, Gordon M. Bingham, John B. Czirr, Hans W. Kruger, and R. E. Shafer, who devoted large amounts of time and energy to this experiment. It is a pleasure to thank Dr. Geoffrey F. Chew, Dr. Richard H. Dalitz, Dr. A. Pais, Dr. Emilo Segrè, and Dr. Kenneth M. Watson for many enlightening discussions. Finally, we wish to thank Mr. James Vale and the entire cyclotron crew for capable and reliable operation of the cyclotron.

---

*This was carried out under the auspices of the U. S. Atomic Energy Commission.

[1]A. Abashian, N. E. Booth, and K. M. Crowe, Phys. Rev. Letters 5, 258 (1960).

[2]A P-wave rather than an S-wave resonance seemed more plausible. See G. F. Chew and S. Mandelstam, Phys. Rev. 119, 467 (1960), footnote 19; W. R. Frazer and J. R. Fulco, Phys. Rev. Letters 2, 365 (1959); Phys. Rev. 117, 1609 (1960).

[3]These data also appear in N. E. Booth, A. Abashian, and K. M. Crowe, Revs. Modern Phys. (to be published) and are available in tabular form in the Lawrence Radiation Laboratory Report UCRL-9599, 1961 (unpublished). Some of the plotted points are slightly in error because of needed corrections that had not been made. The tabulated data, however, have been corrected.

[4]This approach was first suggested to us by Dr. Kenneth M. Watson of this Laboratory as one of several different explanations. Recently, Truong has succeeded in fitting some of our earlier data this way. See T. N. Truong, postdeadline paper at the New York Meeting of the American Physical Society, February, 1961, and Phys. Rev. Letters 6, 308 (1961).

[5]K. M. Watson, Phys. Rev. 88, 1163 (1952).

[6]G. F. Chew and S. Mandelstam, Phys. Rev. 119, 467 (1960).

[7]G. F. Chew, S. Mandelstam, and H. P. Noyes, Phys. Rev. 119, 478 (1960).

[8]G. F. Chew and S. Mandelstam, Nuovo cimento 19, 752 (1961).

[9]B. Desai, Phys. Rev. Letters 6, 497 (1961). Desai has calculated the enhancement factors to be expected if the resonance parameters are assumed to be $\nu_R=3.5$ and $\Gamma=0.3$. With these values, our $a_{S0}=2.5$ gives $\lambda=-0.19$. For the S-dominant case, Eq. (8) gives $\lambda=-0.21$. Recently Moffat and Bransden have obtained

numerical solutions in terms of the single parameter λ. For $\lambda = -0.20$ they calculate $\nu_R = 3.9$, $\Gamma = 0.6$, and $a_{s0} = 2.0$; J. W. Moffat and B. H. Bransden (private communication).

[10]Y. Nambu, Phys. Rev. 106, 1366 (1957).

[11]R. M. Sternheimer and S. J. Lindenbaum, Phys. Rev. 109, 1723 (1958); J. G. Rushbrooke and D. Radojičić, Phys. Rev. Letters 5, 567 (1960).

[12]M. Stearns and M. B. Stearns, Phys. Rev. 103, 1534 (1956).

[13]G. Goldhaber, S. Goldhaber, W. Lee, and A. Pais, Phys. Rev. 120, 300 (1960).

ERRATA

EVIDENCE FOR A π-π RESONANCE IN THE $I=1$, $J=1$ STATE. A. R. Erwin, R. March, W. D. Walker, and E. West [Phys. Rev. Letters 6, 628 (1961)].

Footnote 3 should contain an additional reference to G. F. Chew and S. Mandelstam, Phys. Rev. 119, 467 (1960). At the end of the text, there should be an additional footnote: [8]It is possible that the effects of large S-wave π-π scattering have been observed by A. Abashian, N. E. Booth, and K. M. Crowe, Phys. Rev. Letters 5, 258 (1960).

PROTON-PROTON INTERACTION. H. Feshbach, E. Lomon, and A. Tubis [Phys. Rev. Letters 6, 635 (1961)].

The last two terms in the square bracket of Eq. (1) for $V_4(r)$ should be

$$-\vec{\sigma}^1 \cdot \vec{\sigma}^2 R_2(\mu r) - S_{12} R_3(\mu r),$$

instead of the same terms with positive signs.

The first two terms in the first square bracket of the expression for $R_1(x)$ just below Eq. (1) should read:

$$\left(\frac{12}{x^2} + \frac{23}{x^4}\right) K_1(2x) \text{ instead of } \frac{12}{x^2} + \frac{23}{x^4} K_1(2x).$$

The first line of p. 636 should have $\xi = 0$ instead of $\xi = 1$, and the second line should have $\xi = 1$ instead of $\xi = 0$.